Article

Cell Stem Cell

A Subset of TREM2$^+$ Dermal Macrophages Secretes Oncostatin M to Maintain Hair Follicle Stem Cell Quiescence and Inhibit Hair Growth

Graphical Abstract

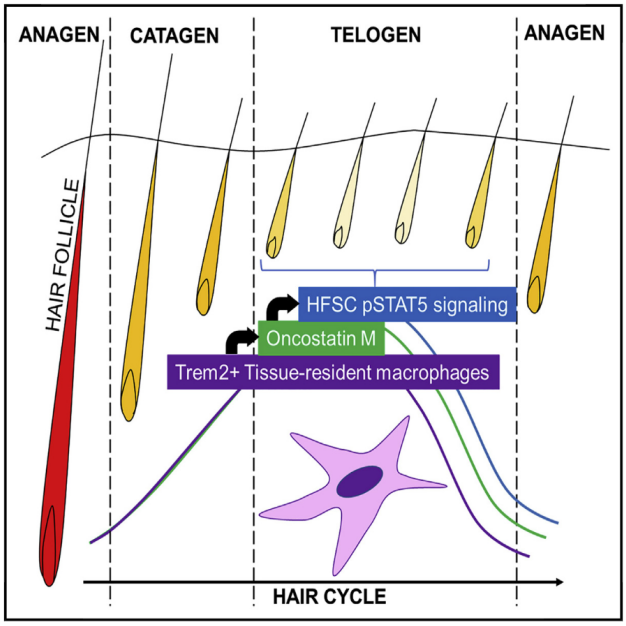

Authors

Etienne C.E. Wang, Zhenpeng Dai, Anthony W. Ferrante, Charles G. Drake, Angela M. Christiano

Correspondence

amc65@columbia.edu

In Brief

Christiano and colleagues show that tissue macrophages secrete Oncostatin M, which activates JAK-STAT5 signaling to maintain hair follicle stem cell quiescence in mice. Targeting these macrophages is associated with stem cell activation, suggesting approaches to managing hair loss in some contexts.

Highlights

- JAK-STAT5 signaling maintains quiescence in hair follicle stem cells (HFSCs)
- Oncostatin M (OSM) acts upstream of JAK-STAT5 signaling to maintain HFSC quiescence
- A subset of TREM2$^+$ macrophages in the mouse skin is the source of OSM
- Specific ablation of macrophages in the mouse skin is associated with anagen entry

Wang et al., 2019, Cell Stem Cell *24*, 654–669
April 4, 2019
https://doi.org/10.1016/j.stem.2019.01.011

CellPress

CellPress

Cell Stem Cell
Article

A Subset of TREM2$^+$ Dermal Macrophages Secretes Oncostatin M to Maintain Hair Follicle Stem Cell Quiescence and Inhibit Hair Growth

Etienne C.E. Wang,[1,5] Zhenpeng Dai,[1] Anthony W. Ferrante,[3] Charles G. Drake,[4] and Angela M. Christiano[1,2,6,*]
[1]Department of Dermatology, Columbia University, New York, NY, USA
[2]Department of Genetics & Development, Columbia University, New York, NY, USA
[3]Institute of Human Nutrition, Columbia University, New York, NY, USA
[4]Herbert Irving Comprehensive Cancer Center, Columbia University, New York, NY, USA
[5]National Skin Center, Singapore, Singapore
[6]Lead Contact
*Correspondence: amc65@columbia.edu
https://doi.org/10.1016/j.stem.2019.01.011

SUMMARY

Hair growth can be induced from resting mouse hair follicles by topical application of JAK inhibitors, suggesting that JAK-STAT signaling is required for maintaining hair follicle stem cells (HFSCs) in a quiescent state. Here, we show that Oncostatin M (OSM), an IL-6 family cytokine, negatively regulates hair growth by signaling through JAK-STAT5 to maintain HFSC quiescence. Genetic deletion of the OSM receptor or STAT5 can induce premature HFSC activation, suggesting that the resting telogen stage is actively maintained by the hair follicle niche. Single-cell RNA sequencing revealed that the OSM source is not intrinsic to the hair follicle itself and is instead a subset of TREM2$^+$ macrophages that is enriched within the resting follicle and deceases immediately prior to HFSC activation. *In vivo* inhibition of macrophage function was sufficient to induce HFSC proliferation and hair cycle induction. Together these results clarify how JAK-STAT signaling actively inhibits hair growth.

INTRODUCTION

The mammalian hair cycle is an exquisitely orchestrated process whereby the hair follicle (HF) undergoes distinct phases of growth (anagen), regression (catagen), and rest (telogen) (Müller-Röver et al., 2001). The keratinocytes of the HFSCs (located in the bulge and secondary hair germ) receive activating signals, such as Wnt and Sonic Hedgehog (Shh), that promote proliferation during anagen, as well as inhibitory signals, such as Bone Morphogenetic Proteins (BMPs), that promote quiescence during telogen (Stenn and Paus, 2001). These molecular cues originate from the hair follicle bulge itself (Hsu et al., 2011), the subjacent dermal papilla (DP), and even exogenous cell types such as adipocytes (Plikus et al., 2008). The hair cycle is also associated with fluctuations in the local immune cell composition (Paus et al., 1998). Recently, macrophages have been shown to increase in numbers during early and mid-telogen (Eichmüller et al., 1998; Castellana et al., 2014), suggesting a role for these cells in the mammalian hair cycle.

A defined role for JAK-STAT signaling in the hair cycle has yet to be established. Constitutive knockout of STAT3 in the epidermis (which includes the HFSCs) results in differential regulation of spontaneous (endogenous) versus induced (exogenous) anagen (Sano et al., 2000). Our lab recently demonstrated that blockade of JAK-STAT signaling during telogen using topical JAK inhibitors was sufficient to induce anagen in resting telogen follicles (Harel et al., 2015), raising the possibility that JAK-STAT signaling is required for maintaining HFSCs in a quiescent state during telogen. While JAK-STAT signaling is generally associated with active processes like proliferation, migration, and differentiation, there is an emerging role for this pathway in promoting stem cell quiescence.

The chalone hypothesis, originally put forth by Claude Bernard in 1878 (Iversen, 1981), suggests that telogen may represent an actively repressed state. Chalones were described as naturally occurring inhibitors of tissue growth and were believed to counter-balance growth and proliferation signals. The presence of a telogen-associated chalone in mouse skin was demonstrated when protein extracts from telogen skin inhibited anagen when injected systemically into other mice (Paus et al., 1990). To date, inhibitory signals during telogen have been attributed to BMP-2 (from the subcutaneous adipocytes) and BMP-4 (from within the hair follicle) (Plikus et al., 2008), as well as BMP-6 and FGF-18 (from the K6$^+$ inner bulge) (Hsu et al., 2011); however, these molecules do not signal through the JAK-STAT signaling pathway and cannot explain the induction of anagen by blocking JAK-STAT signaling.

The potential upstream signal for JAK-STAT-mediated quiescence during telogen can be narrowed down to a family of cytokines that signal through the JAK-STAT signaling and have been shown previously to perturb the hair cycle. Oncostatin M (OSM) was shown to inhibit plucking-induced anagen (Yu et al., 2008), while interleukin-6 (IL-6) could induce catagen in anagen follicles (Kwack et al., 2012). Both OSM and IL-6 belong to the gp130-dependent family of cytokines, which also includes leukemia inhibitory factor (LIF), cardiotrophin-1 (CT-1), ciliary

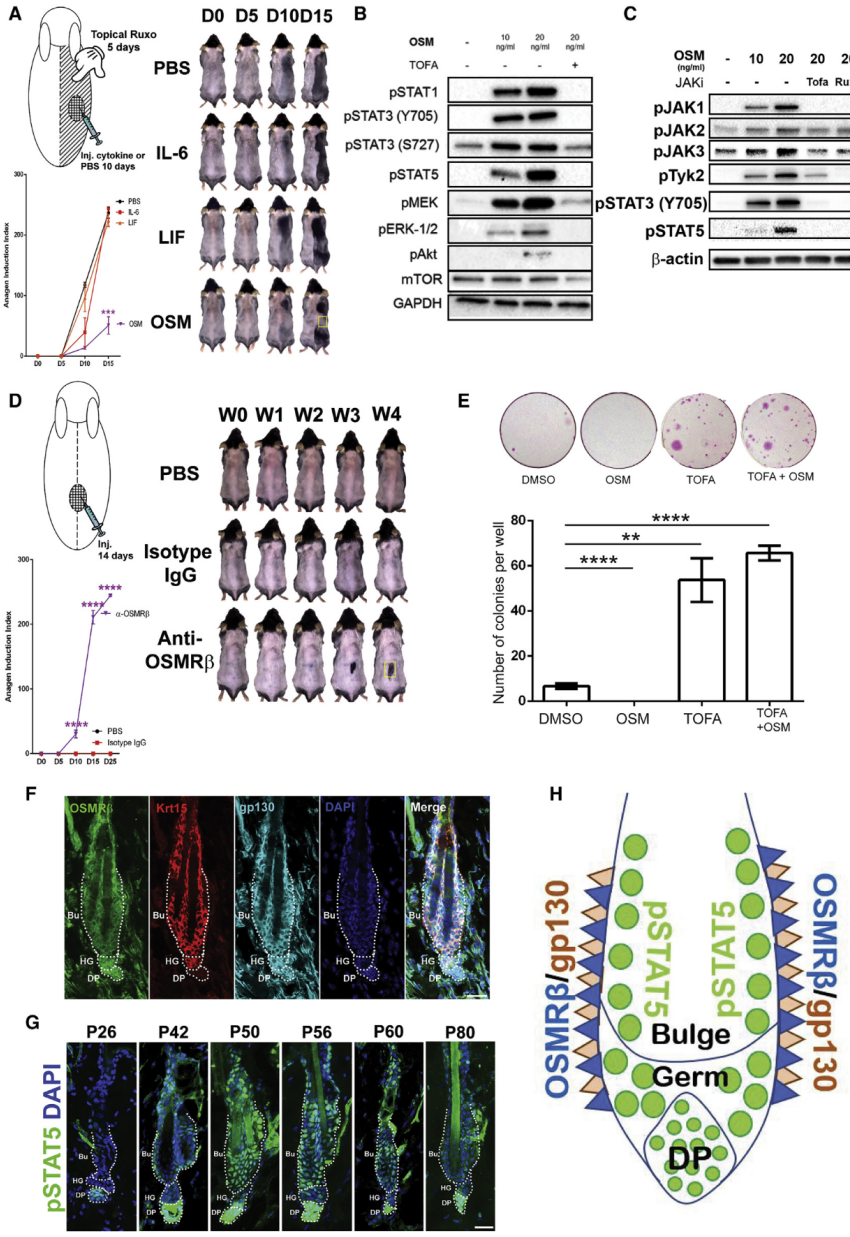

Figure 1. OSM Prevents HFSC Proliferation via OSMR-JAK-STAT5 Signaling

(A) OSM, and not IL-6 or LIF, prevents ruxolitinib-induced anagen. Topical ruxolitinib was applied for 5 days from P60, and cytokines were injected intradermally for an additional 5 days after (for a total of 10 days). Note that the reflective sheen of the fur on the LIF-injected mouse is distinct from the pink hairless skin of the OSM-injected mouse. Data are representative of 2 experiments with n = 4 mice per group.

(legend continued on next page)

neurotrophic factor (CNTF), and others. In addition to the JAK-STAT pathway, this family of cytokines also signals via the MAPK (mitogen-activated protein kinase), mTOR (mammalian target of rapamycin), and PI3K (phosphatidylinositol-3 kinase) pathways, to regulate a variety of biological processes, most notably, stem cell maintenance and quiescence in a variety of tissue types (Rose-John, 2018; Müller-Newen, 2003; Rose and Bruce, 1991).

In this study, we found that OSM inhibits JAK-inhibitor-induced hair growth and thus may represent an endogenous chalone that maintains telogen. We also show that OSM is sufficient for maintaining quiescence of hair follicle stem cells (HFSCs), and JAK-STAT5 signaling via the OSM receptor (OSMRβ) is necessary for maintaining telogen, since conditional ablation of OSMRβ or STAT5 in the epidermis shortens the telogen phase significantly. Using single-cell RNA sequencing, we identified the source of OSM to be a distinct subset of TREM2$^+$ macrophages that predominates during early telogen. Moreover, we found that inhibition of macrophages during telogen by genetic ablation, neutralizing antibodies, and small-molecule inhibitors was sufficient to induce anagen. Hair growth and proliferation of HFSCs were associated with depletion of TREM2$^+$ macrophages, which are spatially, temporally, and functionally relevant for HFSC quiescence during telogen.

RESULTS

OSM Maintains Hair Follicles in Telogen via OSMR-JAK-STAT Signaling

We previously established that spontaneous anagen can be induced by transient topical application of JAK inhibitors for 5 days during mouse telogen (Harel et al., 2015). We tested whether OSM and other gp130 cytokines (IL-6 and LIF) could inhibit the anagen induced by topical JAK inhibitors (Harel et al., 2015) (Figure 1A). OSM, IL-6, LIF, or PBS control was injected intradermally into the middle of the field of topical ruxolitinib 2% application for 10 days (5 days after stopping topical treatment). Intradermal OSM was the only member of the gp130-dependent class of cytokines that inhibited anagen locally in the area where it was administered (Figure 1A), identifying OSM as a candidate upstream factor for JAK-STAT signaling that maintains HFSC quiescence.

Next, we interrogated the OSM signaling pathways in HFSCs. ITGA6$^+$ Sca-1$^-$ HFSCs were isolated from telogen skin by fluorescence-activated cell sorting (FACS), cultured, and stimulated with OSM for 15 min. OSM displayed a dose-dependent activation of the JAK-STAT1, JAK-STAT3, JAK-STAT5, and MAPK-ERK pathways in cultured HFSCs *in vitro* (Figure 1B). OSM had minimal effects on the PI3K-Akt-mTOR pathway. Pre-treatment of cultured HFSCs with Tofacitinib abrogated JAK-STAT and MAPK-MEK-ERK signaling, and, to a lesser extent, PI3K-Akt signaling. Immunofluorescence of pSTAT1 *in vivo* during telogen places its activity in the IFE, isthmus and infundibulum of the telogen hair follicle, and not the bulge and/or hair germ (Figure S1A), making the JAK-STAT1 pathway an unlikely contributor to HFSC quiescence.

We utilized increasingly specific JAK inhibitors to dissect the signaling downstream of OSM. OSM signaling occurs through all four JAK kinases (JAK1, JAK2, JAK3, and Tyk2) (Figure 1C). These pathways were blocked with pre-treatment with Tofacitinib (pan-JAK inhibitor), Ruxolitinib (JAK-1/2 inhibitor), or PF-06651600 (a covalent JAK3 inhibitor). We found that, while different JAK inhibitors had varying effects on JAK1/2/3/Tyk2 and STAT3 phosphorylation, all of them resulted in potent pSTAT5 inhibition (Figure 1C). Notably, the covalent JAK3 inhibitor PF-06651600-initiated anagen with the 5-day topical treatment regimen previously described (Figure S1B), without significant inhibition of STAT3 phosphorylation in HFSCs. This led us to conclude that inhibition of STAT5 phosphorylation (and not STAT3) in HFSCs was sufficient to promote anagen initiation in mid-telogen skin.

Next, we postulated that inhibition of OSM receptor signaling should induce anagen via the same mechanism. First, we confirmed that antibodies to the extracellular domain of OSMRβ was able to abrogate JAK-STAT5 signaling in

(B) OSM activates JAK-STAT1/3/5 pathways and the MAPK-MEK-ERK pathways in cultured HFSCs. Pre-treatment with 10 μM Tofacitinib (Tofa) inhibited the JAK-STAT and, to a lesser extent, the MAPK-MEK-ERK pathways. Total protein levels were not expected to change with short treatment times and are not shown. Data are representative of 3 biological replicates, with representative blots cropped, marked with solid lines.

(C) Western blot of cultured HFSCs stimulated with OSM for 15 min, with or without pre-treatment with JAK inhibitors. OSM had a dose-dependent activation of all four JAKs (JAK1, JAK2, JAK3, Tyk2), as well as pSTAT3 and pSTAT5. Tofacitinib and Ruxolitinib pre-treatment inhibited phosphorylation of a variety of JAKs, and inhibited both pSTAT3 and pSTAT5 activation. PF-06651660, a specific covalent inhibitor of JAK3, did not have an effect on JAK1/JAK2/Tyk2 or STAT3 phosphorylation but still inhibited pSTAT5 activation. All JAK inhibitors for short-term treatments were used at 10 μM. Data are representative of 3 biological replicates.

(D) Intradermal injections of neutralizing antibodies to OSMRβ into the center of the telogen back skin in P60 C57BL/6 mice for 14 days was sufficient to induce local anagen, while injection of PBS and isotype IgG control antibody had no effect. Data are representative of 3 experiments with n = 3 mice per group.

(E) Clonogenicity assays of HFSCs. ITGA6$^+$ Sca-1$^-$ epidermal stem cells were isolated by FACS, plated in 6-well plates, and cultured for 2 weeks. Addition of OSM 10 ng/mL to the culture media completely prevented growth of any stem cell colonies, whereas the addition of Tofacitinib 100 nM enhanced HFSC clone numbers and reversed the effect of OSM. Data are pooled from 3 experiments, with representative plates pictured in the top panel.

(F) Immunofluorescence of P60 telogen hair follicle showing co-localization of OSMRβ and gp130 in the HFSC compartment, marked with the stem cell marker Keratin 15. Note that gp130 expression is ubiquitous. OSMRβ expression is also expressed in scattered dermal cells. Bu, bulge; HG, secondary hair germ; DP, dermal papilla. Scale bar, 25 μm.

(G) Immunofluorescence of pSTAT5 across the hair cycle. Activation of pSTAT5 localizes to the HFSC compartments (bulge and hair germ) particularly strongly from P42–P60, which represents early-to-mid second telogen, and is diminished in the first telogen (P26) and late second telogen (P80), when the hair follicle is ready to enter the next anagen phase. Bu, bulge; HG, secondary hair germ; DP, dermal papilla. Scale bar, 25 μm.

(H) Schematic of OSMRβ/gp130/pSTAT5 expression in telogen HFs. OSMRβ and gp130 are preferentially expressed on the HFSCs. pSTAT5, while constitutively active in the DP throughout telogen, has the most prominent expression in the HFSCs during early-to-mid telogen.

Data are mean ± SEM. *$p < 0.05$, **$p < 0.01$, ***$p < 0.001$, ****$p < 0.0001$, Student's unpaired t test.

cultured HFSCs (Figure S1C). Intradermal injection of these blocking antibodies to OSMRβ at P60 resulted in robust local anagen induction at the site of injection (Figure 1D). This effect was not observed with intradermal PBS or isotype immunoglobulin G (IgG) control.

To show that OSM had direct inhibitory effects on HFSC proliferation, we performed clonogenicity assays with isolated ($ITGA6^+$ $Sca\text{-}1^-$) HFSCs in the presence of OSM (10 ng/mL), Tofacitinib (100 nM), or both (Figure 1E). OSM inhibited HFSC colonies from forming *in vitro*. Tofacitinib increased both the colony-forming ability of HFSCs, and colony size, consistent with previous reports (Doles et al., 2012). Addition of Tofacitinib was also sufficient to abrogate the inhibitory effects of OSM when both were continually present in the culture medium. These results suggest that OSM acts via JAK-STAT signaling, most likely via activation of STAT5, to prevent proliferation of HFSCs, and is sufficient for preventing HFSC proliferation and maintaining their quiescence during telogen in mouse skin.

OSMRβ and Its Co-receptor gp130 Co-localize with Activated pSTAT5 in Bulge and Germ HFSCs during Early and Mid-telogen

In the mouse, OSM binds specifically to its receptor OSMRβ, which requires the co-receptor gp130 for signaling via the JAK-STAT pathway (Gómez-Lechon, 1999). By separating the mouse dorsal skin into the epidermal and dermal compartments and performing quantitative real-time PCR for OSMRβ and OSM, we showed that OSMRβ was distinctly expressed in the total epidermal fraction (which contains the epithelial parts of hair follicles), and OSM was expressed in the total dermal fraction (which contains the dermal cells and the DP) (Figure S1D).

To further define the expression of OSMRβ and gp130 in the epidermis, the epidermal fraction was separated by FACS into the $Sca\text{-}1^+$ interfollicular epidermis (IFE), $CD34^+$ bulge, and the P-$cadherin^+$ hair germ. Quantitative real-time PCR for Keratin 17 (a differentiated hair follicle keratin) validated this sorting strategy with increasing expression of Krt17 from IFE > Bulge > hair germ (Figure S1E). Quantitative real-time PCR showed that OSMRβ and gp130 were preferentially expressed in the bulge and hair germ telogen HFSCs. This was confirmed with immunofluorescence (Figure 1F).

Activated pSTAT5 was found to be significantly expressed in both the DP and the HFSCs during telogen (Figures S1F and S1G) (Harel et al., 2015). Western blots showed that activated pSTAT5 protein is also dynamically expressed in the epidermis across telogen, peaking at mid-telogen around P56-P60 (Figure S1H). Using immunofluorescence, we showed that pSTAT5 during early and mid-telogen is localized prominently in the bulge and hair germ HFSCs (Figure 1G). pSTAT5 expression in the HFSC decreases by the end of telogen (P80), in agreement with recent publications (Flores et al., 2017). The peak of pSTAT5 activity in the HFSC during mid-telogen coincides with a peak of OSM expression in the dermis, measured with quantitative real-time PCR (Figure S1I). These data are consistent with the existence of a dermal-epidermal signaling axis whereby dermal OSM signals via OSMRβ-pSTAT5 in HFSCs during early and mid-telogen (Figure 1H), and this signaling decreases during late telogen.

Genetic Ablation of OSMRβ Signaling Shortens the Second Telogen

Next, we used genetic mouse models to disrupt OSM-OSMRβ-STAT5 signaling, postulating that it would impact HFSC quiescence or proliferation. We crossed C57BL/6 mice with *K5-CreERT$_2$* transgenes to either *OSMRβ$^{FL/FL}$* or *STAT5a/b$^{FL/FL}$* mice. Intraperitoneal tamoxifen given during early-to-mid telogen significantly reduced OSMRβ or STAT5 expression in the $K5^+$ epidermis, which includes the HFSC and was confirmed with quantitative real-time PCR, western blot, and immunofluorescence studies (Figures S2A–S2E). Mice were closely shaved with clippers (without injuring the skin) to allow for direct visualization of the dorsal skin, which appears uniformly pink during the synchronized second telogen (P45–P100) and darkens upon entry into anagen when melanocytes proliferate. Epidermal OSMRβ ablation was associated with loss of pSTAT5 signaling in HFSCs during telogen (Figure S2C), without affecting pSTAT5 signaling in the DP (which is K5-negative).

Ablation of epidermal OSMRβ or STAT5 at P35–P38 (end of anagen) was associated with a second telogen that lasted only 2 weeks, shortened from the typical 40–60 days in the C57BL/6 mouse (Figure 2A). *K5-CreERT$_2$::OSMRβ$^{FL/FL}$* and *K5-CreERT$_2$::STAT5a/b$^{FL/FL}$* mice did not enter full telogen as did their wild-type littermates (Figure 2B). At P60, when control littermates were in telogen, both homozygous mutant mice for *OSMRβ* and *STAT5a/b* were in anagen (Figure 2C). This strongly suggests that OSMRβ signaling, likely via STAT5a/b, in HFSCs during early telogen is necessary for establishing quiescence of HFSCs.

Genetic Ablation of OSMRβ and STAT5 during Mid-telogen Promotes HFSC Proliferation and Anagen Initiation

We next used genetic models to recapitulate the pharmacological effect of JAK inhibition in mouse mid-telogen skin. Tamoxifen induction was carried out during mid-telogen (P53–P60). Both *K5-CreERT$_2$::OSMRβ$^{FL/FL}$* and *K5-CreERT$_2$::STAT5a/b$^{FL/FL}$* mice entered anagen significantly earlier than control littermates (Figures 2D and 2E), approximately 3 weeks after tamoxifen induction. Genetic ablation of OSMRβ or STAT5 in the epidermis and hair follicle later than P60 did not result in significantly earlier anagen induction (data not shown), suggesting quiescence mediated by OSMRβ-JAK-STAT5 signaling is more physiologically relevant during early and mid-telogen.

We next studied the cellular dynamics that result from genetic ablation of STAT5 in the HFSCs. Cellular proliferation was studied at 10 and 20 days (D10 and D20) post-tamoxifen with 5-ethinyl-2'-deoxyuridine (EdU) administration 24 hr before the mice were sacrificed. At D10 post-tamoxifen induction, cellular proliferation was observed in the hair germ, while the bulge remained quiescent (Figure 2F). At D20, the proliferation in the hair germ was even more prominent, and EdU incorporation was also seen in the lower bulge (Figure 2G).

We utilized flow cytometry of HFSCs to examine the responses of the bulge and hair germ to STAT5 ablation (Figure S3A). We found that the P-$cadherin^+$ hair germ population nearly doubles at D10 (Figure 2H), whereas the $CD34^+$ bulge population remains constant. This difference is more striking

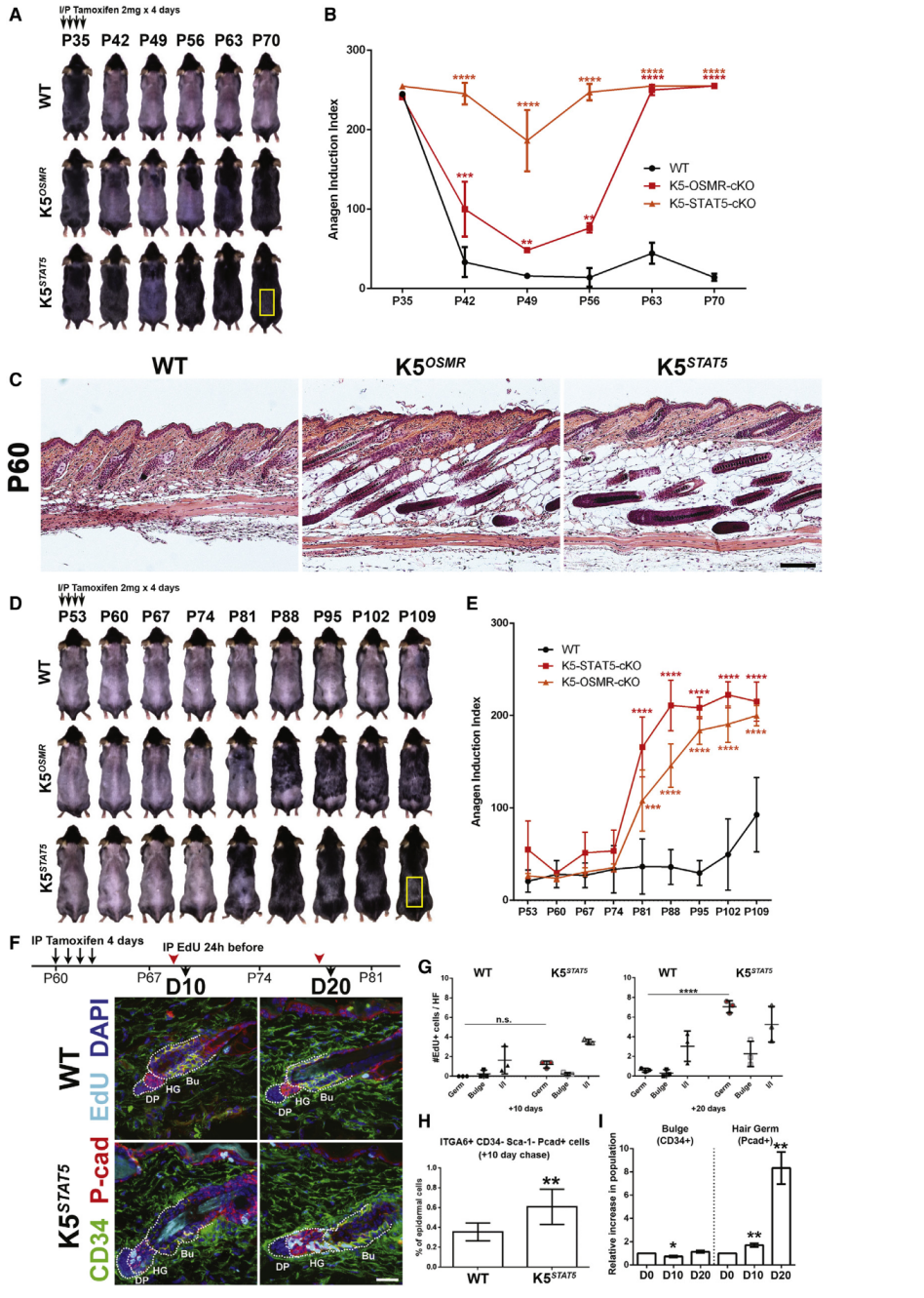

(legend on next page)

by D20, whereby the hair germ proliferates up to 8-fold while the cell numbers of the bulge stay constant (Figure 2I).

To further interrogate the responses of bulge and hair germ HFSCs with STAT5 ablation, we performed clonogenicity assays on epidermal stem cells from WT and *K5-CreERT$_2$::STAT5a/b$^{FL/FL}$* mice. Sca-1$^+$ IFE, CD34$^+$ bulge, and P-cadherin$^+$ hair germ stem cells were isolated by FACS and cultured for 2 weeks, as described earlier, with or without 100 nM Tofacitinib (Figures S3B and S3C). IFE colony-forming ability was minimally affected by both STAT5 ablation and JAK inhibition. Cultured bulge cells were only responsive to JAK inhibition and not influenced by STAT5 ablation. Increased clonogenicity was observed in hair germ cells with both STAT5 ablation and JAK inhibition. These data support the hypothesis that bulge and hair germ HFSCs have intrinsic differences and maintain quiescence via distinct signaling mechanisms, consistent with the proposed two-step model of HFSC activation during anagen (Greco et al., 2009).

Dermal OSM Is Produced by Tissue-Resident Macrophages during Telogen

In order to define the source of dermal OSM, we performed quantitative real-time PCR on isolated dermal tissue collected across different time points in the murine hair cycle. Dermal OSM expression peaked in mid-telogen (Figure S1I). As the human DP may be the source for IL-6 (Yu et al., 2008), we employed laser-capture microdissection (LCM) to isolate the DP to locate *Osm* transcripts (Figure S3D). Perifollicular dermal tissue, primarily containing dermal fibroblasts (DF) but not DP, was used as a control. While DP-specific LEF1 was found in the DP, and COL1A1 was found enriched in both dermal populations as expected, no OSM expression was detected (Figure S3E).

We referred to Hair-GEL.net, an comprehensive online resource for gene expression profiles of sorted mouse skin compartments at post-natal day 5 (P5) (Sennett et al., 2015; Rezza et al., 2016). While OSMRβ and gp130 expression were confirmed to be expressed in HFSCs, OSM was expressed in the "Neg" population of skin cells, which includes immune cells, smooth muscle cells, and endothelial cells of the dermis.

We postulated that OSM might be produced by tissue macrophages, since they have been shown play a role in maintaining the second murine telogen (Castellana et al., 2014). Using FACS, we sorted the telogen dermis for macrophages (F4/80$^+$ CD11b$^+$) (Figure 3A). Using quantitative real-time PCR, the non-macrophage immune cells (CD45$^+$ F4/80$^-$ CD11b$^-$) and DP (CD45$^-$ ITGA9$^+$, identified using the online resource Hair-GEL.net (Sennett et al., 2015; Rezza et al., 2016)) were mostly negative for OSM. By quantitative real-time PCR, macrophages (CD45$^+$ F4/80$^+$ CD11b$^+$) were found to be the main source of dermal OSM (Figure 3B). Using CD163 and major histocompatibility complex (MHC) II as markers for tissue-resident, anti-inflammatory "M2-like" and inflammatory "M1-like" markers, respectively, we found OSM to be enriched in the anti-inflammatory CD163$^+$ MHC II^{low} macrophage subset (Figure 3C).

Macrophage-Derived OSM Inhibits HFSC Proliferation *In Vivo*

Next, we used *in vivo* hair reconstitution assays to examine the interaction between macrophage-produced OSM and HFSCs. Briefly, dissociated neonatal keratinocytes and dermal cells from C57BL/6 pups were mixed into a slurry and injected intradermally into a *nude* mouse. This patch assay recapitulates the epithelial-mesenchymal interactions required for hair follicle regeneration. Tofacitinib enhanced the hair follicles generated in this assay, consistent with our previous findings (Harel et al., 2015), and addition of OSM completely inhibited hair reconstitution. When dermal macrophages were recombined with the

Figure 2. Genetic Ablation of OSMRβ and STAT5 in the Epidermis during Telogen Is Sufficient to Initiate Anagen

(A and B) Conditional knockout of either the *OSMRβ* or the *STAT5* gene using the *K5-CreERT$_2$* driver before the early telogen resulted in a significantly shortened telogen phase (A). STAT5 ablation during catagen prevented HFSC from reaching full quiescence. Anagen progression was quantified as described earlier (B). Results are representative of 3 litters (both males and females) for each gene (*OSMRβ* or *STAT5*), with 2–5 mice per litter, for a total of 10 mice for *OSMRβ* (3 homozygous *OSMRβ$^{FL/FL}$*) and 11 mice for *STAT5* (3 homozygous *STAT5$^{FL/FL}$*).

(C) Histological H&E examination of WT, *K5-CreERT$_2$::OSMRβ$^{FL/FL}$* mice. *K5-CreERT$_2$::OSMRβ$^{FL/FL}$* mice that underwent tamoxifen induction at P35-P38. At P60, when WT littermates were well into telogen, mice lacking *OSMR* or *STAT5* in their epidermal compartments were well into their next anagen phase, accompanied by the thickening of the adipose tissue. Scale bar, 100 μm.

(D and E) Conditional knockout of *OSMRβ* or the *STAT5* at P56-P60 (mid-telogen) resulted in early anagen initiation (*K5^{OSMR}* or *K5^{STAT5}*) compared to control littermates (D). Anagen progression was quantified as described earlier (E). Results are representative of 4 litters for each gene (*OSMRβ* or *STAT5*), with 2–4 mice per litter, for a total of 11 mice for *OSMRβ* (4 homozygous *OSMRβ$^{FL/FL}$*) and 12 mice for *STAT5* (4 homozygous *STAT5$^{FL/FL}$*). Results were similar in both male and female mice.

(F) EdU incorporation was analyzed +10 and +20 days (D10 and D20) after tamoxifen induction at P60 in *K5-CreERT$_2$::STAT5$^{FL/FL}$* mice. EdU (4 mg/25 g adult mouse) was injected 24 h before sacrifice. At D10 after STAT5 epidermal ablation, EdU incorporation is seen in the hair germ, while the bulge remained quiescent. At D20, while occasional EdU$^+$ cells were seen in the bulge, the hair germ was even more proliferative. Images are representative of 3 biological replicates. Bu, bulge; HG, secondary hair germ; DP, dermal papilla. Scale bar, 25 μm.

(G) Quantification of proliferative cells (EdU$^+$) in each hair follicle compartment: P-cad$^+$ hair germ, CD34$^+$ bulge, or isthmus and/or infundibulum (I/I) after tamoxifen induction of STAT5-ablation in WT and *K5-CreERT$_2$::STAT5$^{FL/FL}$* littermates. CD34-negative cells above the bulge but within the hair follicle were considered I/I. EdU incorporation was observed in the hair germ by D10 (n.s.), which became significant by D20. At D10, bulge proliferation was minimal, and slightly increased at D20. (Data points are mean of 20 HFs per mouse, n = 3 mice per genotype.)

(H) Flow cytometric quantification of stem cell populations. At D10 after STAT5 ablation, the percentage of total ITGA6$^+$ Sca-1$^-$ CD34$^-$ Pcad$^+$ cells (hair germ) approximately doubled. (Pooled data are from n = 3 mice per genotype.)

(I) While the cell population in the bulge remained relatively constant after epidermal STAT5 ablation, the hair germ proliferated and expanded exponentially with the loss of STAT5 signaling. (Pooled data are from n = 3 mice per genotype.)

Data are mean ± SEM. *p < 0.05, **p < 0.01, ***p < 0.001, ****p < 0.0001, in (B), (E), and (I), two-way ANOVA between genotypes at each respective time point; (G) two-way ANOVA of cellular compartment between genotypes at D10 and D20. (H) Student's t test.

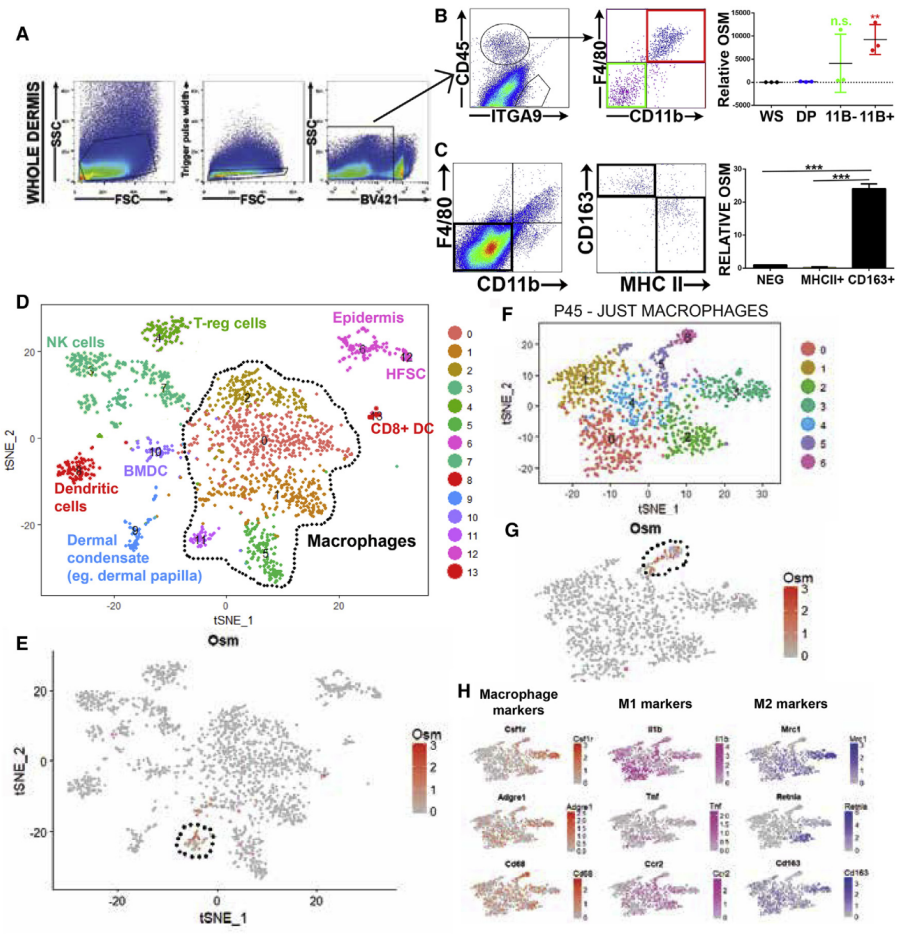

Figure 3. Macrophages Are the Source of OSM in the Dermis

(A and B) Flow cytometric analysis of P50 telogen dermis to isolate macrophages ($CD45^+$ $F4/80^+$ $CD11b^+$) out of whole skin (WS) (A). Quantitative real-time PCR for OSM revealed that dermal macrophages ($F4/80^+$ $CD11b^+$, "$11B^+$") were the main source of OSM (B). DPs ($CD45^-$ Integrin $\alpha9^+$) and $CD11b^-$ "11B-" immune cells were generally negative for OSM. Percentages out of total dermal cells. (Data are pooled from n = 3 mice.)

(C) Flow cytometric analysis of "M1-like" inflammatory (MHC II^+) and "M2-like" non-inflammatory ($CD163^+$) macrophages during telogen (from $CD45^+$ $F4/80^+$ $CD11b^+$ subset). Quantitative real-time PCR of macrophage subsets isolated by this FACS strategy confirmed that $CD163^+$ non-inflammatory macrophages were the main source of OSM in the dermis. Percentages out of total dermal cells. "Neg" cells represent $CD45^+$ $F4/80^-$ $CD11b^-$ non-macrophage immune cells. (Data are pooled from n = 3 mice.)

(D and E) Single-cell RNA sequencing of $CD45^+$ dermal immune cells at P45 (early telogen). $CD45^+$ cells were isolated with flow cytometry and analyzed using the 10x Genomics platform (N = 2,145 cells) (D). Computational analysis was performed using the Seurat R package. Macrophages (defined by CD68, Csf1r, F4/80) clustered into 5 distinct clusters (0, 1, 2, 5, 11, circled with dotted line in D). OSM was enriched in cluster 11 (E). Other clusters were identified according to their gene expression, and these yielded T-reg cells (4), NK cells (3, 7), dendritic cells (8, 13), dermal-condensate cells likely corresponding to dermal papilla (9), bone-marrow derived mesenchymal stem cells (BMDCs, 10), and keratinocyte contaminants (6, 12). Gene expression of each cluster can be found in Table S1.

(F and G) Clustering of just the macrophage populations yielded seven distinct subsets (F), with OSM production enriched in cluster 6 of this re-analysis (dotted circle in G).

(H) Visual inspection of known macrophage markers and inflammatory or anti-inflammatory (M1-like/M2-like) markers show that there is significant heterogeneity of macrophages in unperturbed mouse telogen skin. Clusters 0 and 1 tend to express more "M1-like" markers, while clusters 2 and 3 expressed more "M2-like" markers. Cluster 6, where OSM is enriched, does not fall clearly into either M1-like or M2-like phenotype based on conventional markers. Note Adgre1 = F4/80; Mrc1 = CD206.

Data are mean ± SEM. *$p < 0.05$, **$p < 0.01$, ***$p < 0.001$, ****$p < 0.0001$, in (A)–(C) one-way ANOVA.

neonatal cells, hair reconstitution was also suppressed (Figure S3F).

Next, we cultured murine peritoneal macrophages in the presence of M-CSF to skew them to a tissue-resident, anti-inflammatory phenotype (Weisser et al., 2013), and short hairpin RNA (shRNA) was utilized to knockdown OSM expression (Figure S3G). While control scrambled shRNA did not have any effect on the inhibitory properties of macrophages in the patch assay, OSM knockdown in macrophages rendered them inert with respect to this assay (Figure S3H). These data strongly suggest that OSM produced by macrophages inhibits proliferation and activation of HFSCs.

Single-Cell RNA Sequencing of Dermal CD45$^+$ Immune Cells

To further define the OSM-producing macrophage subset *in vivo*, we performed an unbiased single-cell RNA sequencing of the dermal CD45$^+$ immune cells during early (P45), mid (P50, P63), and late (P80) telogen. This analysis during early telogen (P45) revealed 13 distinct clusters (Figure 3D), which represent the main components of the immune infiltrate in unperturbed mouse early telogen skin. Using established macrophage markers CD68, F4/80 (Adgre1), and Csf1r (Martinez-Pomares et al., 1996; Sasmono et al., 2003), we found that P45 macrophages were organized into 5 distinct clusters: 0, 1, 2, 5, and 11 (Figure S4A). OSM itself was significantly upregulated in a distinct cluster (cluster 11) (Figure 3E).

We re-analyzed the data focusing exclusively on the macrophage clusters to produce a new set of 7 clusters (Figures 3F and 3G). These macrophage-only clusters showed relatively uniform CD68 expression but were heterogenous with respect to classic inflammatory and anti-inflammatory markers (Figure 3H). Cluster 3 macrophages were relatively enriched for anti-inflammatory markers Mrc2 (CD206) and CD163, while clusters 0 and 1 expressed inflammatory markers like IL-1b and MHC class II (H2-Ab1).

OSM expression was almost exclusively restricted to cluster 6 macrophages after this re-analysis (Figure 3G), which did not conform to either a classic inflammatory (“M1-like”) or anti-inflammatory (“M2-like”) gene expression profile.

OSM-Producing Macrophages Are TREM2$^+$ and Have a Distinct Gene-Expression Profile

The most upregulated genes in each macrophage cluster were expressed in a heatmap in order to define the molecular characteristics of OSM-producing macrophages. Cluster 6 macrophages most resembled the “M2-like” macrophages of cluster 3 (Figure 4A). Interestingly, TREM2 was found to be a distinguishing marker between these two subsets and was highly expressed by cluster 6 OSM-producing macrophages, but not expressed in cluster 3 macrophages.

Analysis of cluster 6 genes (Figure S4B) with the online resource Enrichr (http://amp.pharm.mssm.edu/Enrichr/) found a molecular signature that was strikingly similar to published gene sets associated with microglia (Figure S4C), which are long-term tissue-resident macrophages of the CNS (Figure 4B). Established microglial markers such as Apoe, Aif-1 (Iba-1), Cx3cr1, and Tmem119 were all expressed at varying levels in the OSM-producing macrophages, while TREM2 was the most specific identifying marker for this set of macrophages (Figure 4C). CCR2, which marks monocyte-lineage immune cells recruited from the blood, was evenly expressed across all the clusters. Analyzing the markers in the macrophage clusters, OSM and TREM2 expression were found to be highly specific for cluster 6 (Figure 4D).

TREM2$^+$ OSM-Producing Macrophages Are Closely Associated with HFSCs

Immunofluorescence was performed on 30 μm sections of mouse dermal skin with markers identified in this distinct subset of macrophages. Aif-1 (expressed in most macrophages at P45) co-localized with CD11b and OSM in immune cells around the hair follicle at P45 (Figure 5A). TREM2 co-localized with F4/80 and OSM in macrophages near telogen HFSCs (Figure 5B). These data strongly suggest that OSM is produced by TREM2$^+$ macrophages that are spatially associated with HFs during telogen.

TREM2$^+$ Macrophages Decrease over Telogen

Next, we postulated that, if TREM2$^+$ macrophages inhibit HFSC proliferation, their numbers would diminish before the next anagen phase. Single-cell RNA sequencing of CD45$^+$ dermal immune cells was performed at 3 other time points during telogen (Figure 5C). We found that the CD45$^+$ immune cell heterogeneity in the dermis decreases as telogen progresses, starting with 13 distinct clusters at P45 and falling to 3 clusters by P63. The OSM-producing cluster, while distinct at P45, becomes less distinct at P50, and is greatly diminished by P63 and P80 (Figure 5D). This was confirmed using flow cytometry, whereby TREM2$^+$ macrophages in the dermis were prominent during early and mid-telogen, and greatly reduced in both proportion and absolute number by late telogen (Figure 5E).

When cells from all telogen time points were pooled and analyzed altogether, the OSM-producing macrophages from P45 cluster distinctly (Figures S5A and S5B), suggesting that these cells are unique to early telogen and are gradually lost as telogen progresses. When the pooled data are labeled according to the 4 telogen time points, early, mid-, and late telogen have overlapping yet quite distinct immune cell profiles (Figure S5C). Cells from the later timepoint are not found in the OSM cluster, supporting the claim that the OSM-producing cluster is distinctly made up of early-telogen cells. In order to correct for cell numbers, the OSM-producing cluster at P45 was still distinct when this dataset was downsampled to 500 cells (data not shown).

Analyzing the trajectories of OSM and microglial markers across telogen, we found that the fraction of cells expressing all of these genes decrease over the course of telogen (Figure S5D). These data support the model whereby TREM2$^+$ macrophages produce OSM during telogen to maintain HFSC quiescence via OSMRβ-STAT5 signaling (Figure 5F).

Macrophage Inhibition during Telogen Leads to Anagen Initiation

Since a reduction of TREM2$^+$ macrophages occurred during the telogen-to-anagen transition, we asked whether we could influence the hair cycle by targeting macrophages specifically. We

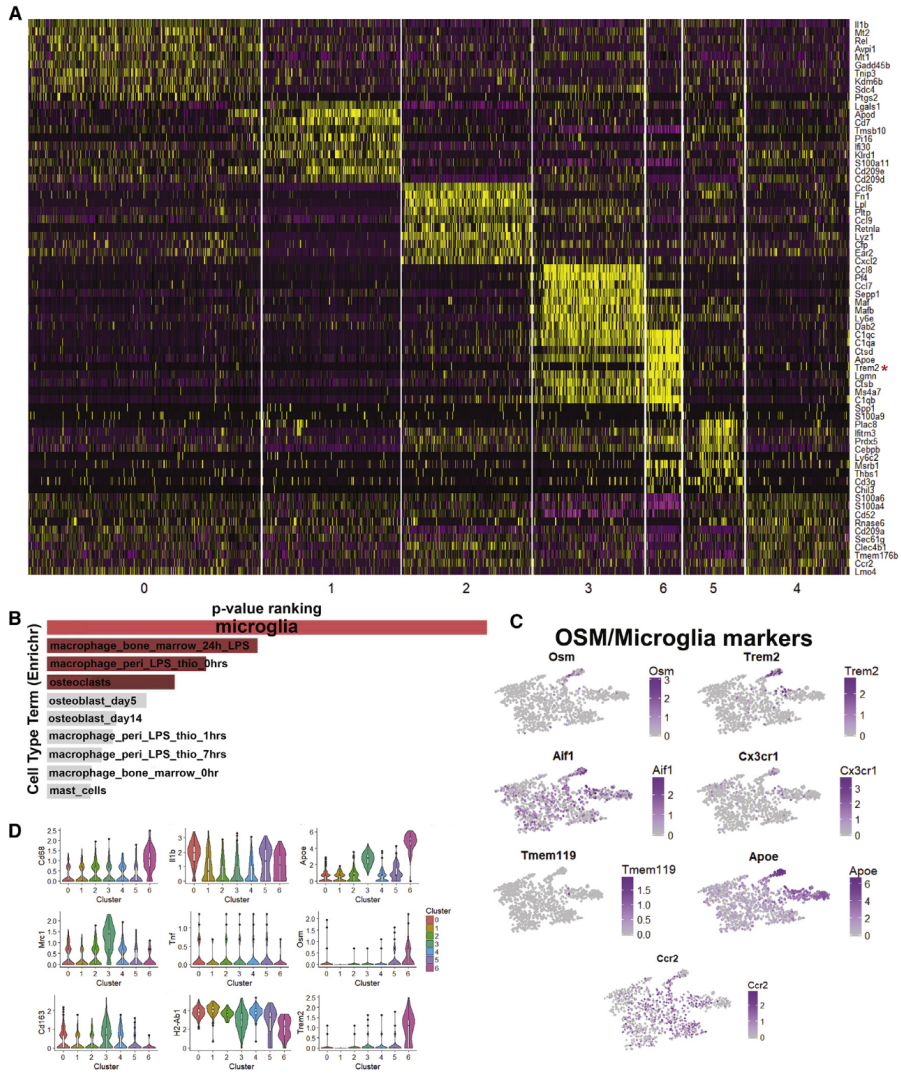

Figure 4. OSM-Producing Macrophages Have a Distinct Gene Expression Profile

(A) Heatmap showing differentially enriched genes in macrophage clusters. The gene expression profile of cluster 6 OSM-producing macrophages resembled M2-like macrophages in cluster 3, except for TREM2 (red asterisk *), which is conspicuously absent in cluster 3. Each column represents a single cell, yellow signifies upregulation, and purple signifies downregulation.

(B) Enrichr analysis of most enriched genes in cluster 6 (Figure S4A) suggests that these genes are also enriched in microglia, according to the Mouse Gene Atlas (Figure S4B).

(C) Classic microglial markers have different distributions among the dermal macrophages, and most are expressed in cluster 6. Note that CCR2, which is expressed on monocyte-lineage cells recruited from the blood circulation, is expressed evenly across all subsets.

(D) Violin plots of gene expression across macrophage subsets. Cluster 3 tends to have more tissue-resident, anti-inflammatory markers (Mrc1 = CD206; CD163), while clusters 0 and 1 are more enriched in inflammatory markers like IL-1b, TNF, and MHC II (H2-Ab1). Microglial markers ApoE and TREM2 are co-expressed in cluster 6 macrophages along with OSM, with TREM2 being the most specific to this population.

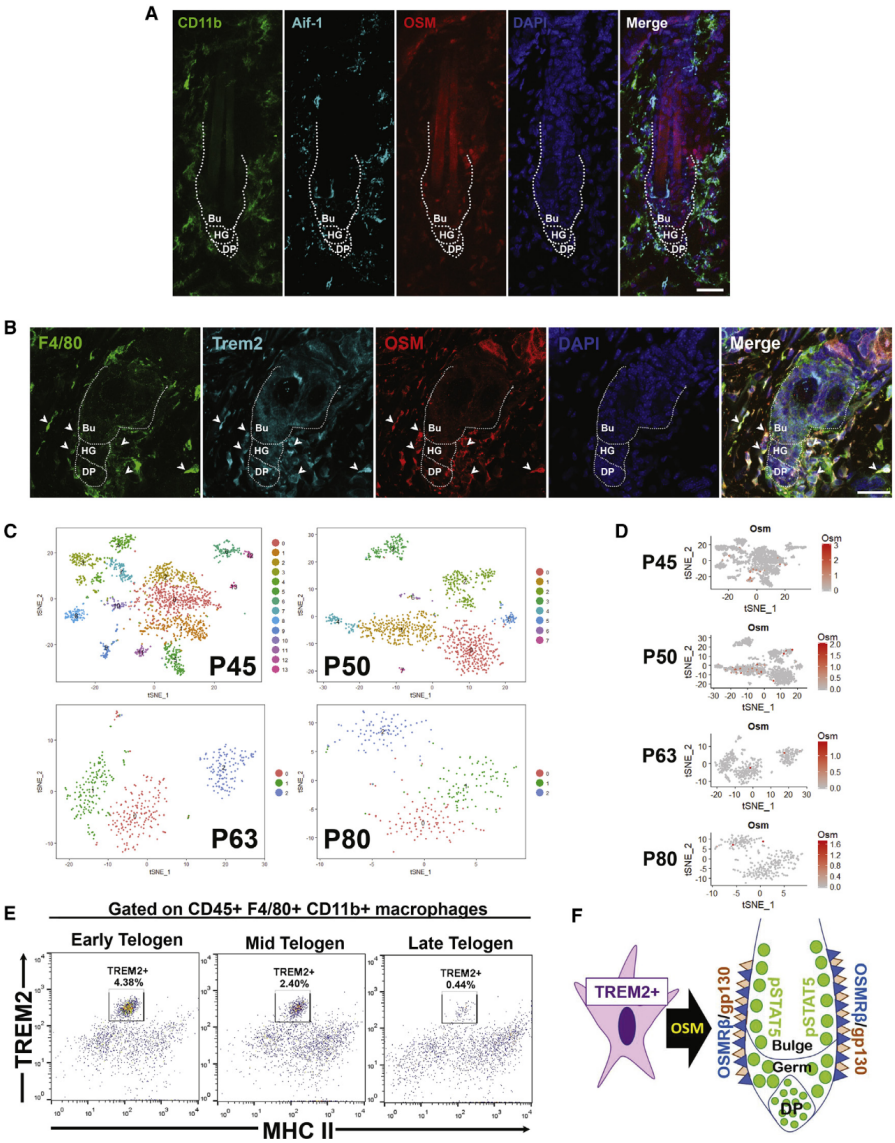

Figure 5. OSM-Producing Macrophages Are Associated with HFs and Disappear during Telogen

(A) Immunofluorescence of Aif-1, a microglial marker, that co-localizes with CD11b and OSM, surrounding a telogen hair follicle at P45. z stack of a thick, 30 μm section is shown. Representative image of n = 3 mice. Bu, bulge; HG, secondary hair germ; DP, dermal papilla. Scale bar, 25 μm.

(B) Immunofluorescence of TREM2, a specific marker for the OSM-producing macrophages, co-localizing with F4/80 and OSM, surrounding the HFSC of a telogen hair follicle. z stack of thick, 30 μm section is shown. Representative image of n = 3 mice. Bu, bulge; HG, secondary hair germ; DP, dermal papilla. Scale bar, 25 μm.

(C) Single-cell RNA sequencing was performed at 3 other time points in telogen (P50, P63, P80). Number of cells at each time point analyzed were 1,497 (P50), 592 (P63), and 497 (P80). Immune cell diversity is diminished as telogen progresses (fewer clusters by late telogen).

(D) The OSM-producing cluster becomes less distinct as telogen progresses. At P50, OSM-producing macrophages are dispersed in the main macrophage cluster, and by P63, very few cells express OSM.

(legend continued on next page)

used three independent methods of macrophage inhibition during telogen to initiate anagen in C57BL/6 mice.

First, we used a genetic ablation model by generating *Csf1r-CreER::Rosa26-iDTR (R26-iDTR)* mice, which express tamoxifen-inducible diphtheria toxin receptors on Csf1r$^+$ cells. Tamoxifen was administered for 4 days in mid-telogen, followed by 7 days of intradermal diphtheria toxin (DTA) injections. This treatment led to ablation of dermal macrophages, which resulted in local anagen (Figure 6A). Introduction of the *R26-TdTomato* reporter allowed us to visualize macrophage ablation in these mice. Drastic reduction in perifollicular TdT$^+$ macrophages was observed in the area of intradermal DTA injection (Figure 6B), which was associated with increased EdU incorporation of HFSCs (Figure 6C). To determine the specificity of the model, we measured the relative ablation of different Csf1r$^+$ positive cells in the dermis (i.e., macrophages and dendritic cells, DCs) after intradermal DTA injection. We showed that, while there was 88% ablation of DCs, macrophages underwent preferential 100% depletion in the dermis (Figures S6A and S6B). Further, quantitative real-time PCR on DCs and macrophages show that TREM2$^+$ macrophages are the main source of OSM, consistent with our single-cell RNA sequencing data (Figure S6C). Flow cytometry of the dermis biopsied from these areas also shows preferential ablation of the F4/80$^+$ TREM2$^+$ subset of macrophages (Figure S7A), which corresponds to the OSM-producing subset. These data are consistent with our hair reconstitution patch assays showing increased hair regeneration with OSM knock-down in macrophages (Figure S3F-H). Intriguingly, the cranio-caudal wave of anagen was also observed to occur earlier in the *R26-iDTR* mice treated with intradermal DTA (Figure 6A), suggesting a possible systemic effect of intradermal DTA injection in this genetic model.

Next, we showed that intradermal injection of neutralizing antibodies to macrophage receptors Csf1r (AFS98) and F4/80/EMR1 (CI:A3-1) during mid-telogen, which have been shown to effectively deplete tissue resident populations of macrophages at the point of administration (MacDonald et al., 2010; Segawa et al., 2008), was able to initiate a local anagen (Figure 6D).

Last, we utilized small-molecule inhibitors of Csf1r. Topical and subcutaneously delivered pexidartinib (PLX3397, Csf1r tyrosine kinase inhibitor) (Figure 6E) was effective at initiating anagen at P60. Since pexidartinib has reported off-target effects, such as inhibitory actions on c-kit, we also tested two other Csf1r inhibitors, BLZ945 and GW2580, which were similarly effective at initiating anagen when applied topically (Figure S7B). As a negative control, we applied the c-kit inhibitor telatinib, which did not initiate anagen when applied topically to P60 telogen skin.

Csf1r and JAK Inhibition Were Specific for Macrophages and HFSCs, Respectively

In order to rule out whether topical JAK inhibitors could be initiating anagen by influencing the dermal TREM2$^+$ macrophages, we showed that 5 days of topical ruxolitinib treatment, which induces anagen by antagonizing JAK-STAT5 signaling in HFSCs, did not have an effect on dermal TREM2$^+$ macrophages (Figure 7A). Further, quantitative real-time PCR of FACS-isolated TREM2$^+$ macrophages showed that topical JAK inhibition led to reduced STAT3 expression, which is both a target gene and component of JAK-STAT3 signaling, had little effect on STAT5 signaling or OSM expression (Figure 7B). These data support our model that JAK inhibitors are working at the level of OSMRβ-JAK-STAT5 in the HFSCs during telogen to maintain quiescence. Small-molecule inhibitors of Csf1r, which might have off-target effects on HFSCs, also did not completely inhibit JAK-STAT5 signaling in HFSCs when compared to tofacitinib (Figure 7C).

We found that Tregs, which have recently been shown to play a role in depilation-induced anagen (Ali et al., 2017), were dispensable for anagen resulting from JAK inhibition or macrophage inhibition using a Csf1r inhibitor (Figures 7D and 7E), which may more closely represent spontaneous anagen.

These findings support our hypothesis that macrophages are necessary for the maintenance of an inhibitory environment on the HFSCs during telogen, via production of OSM (Figure S7C).

DISCUSSION

In this study, we uncovered a distinct role for JAK-STAT signaling in the maintenance of HFSC quiescence. We identified OSM as a negative regulator of hair growth that maintains HFSC quiescence via JAK-STAT5 signaling *in vivo*. Unexpectedly, we discovered a distinct subset of TREM2$^+$ dermal macrophages that secretes OSM, which prevents proliferation of HFSC and inhibits hair growth during telogen (Figure 5F). These macrophages are genetically distinct (Figure 3E), express markers that are associated with long-term resident microglia of the CNS (Figure 4), and are spatially and temporally associated with early telogen HFs (Figure 5). Depletion of this subset of macrophages is associated with the induction of hair growth in mice (Figure 6), making them functionally unique. We propose the name "trichophages" to refer to these specialized macrophages that maintain HFSC quiescence during telogen.

In previous studies, macrophages were shown to cluster around hair follicles (Eichmüller et al., 1998), and may secrete factors such as FGF-5 that promotes catagen (Suzuki et al., 1998, 2000). Castellana et al. showed that macrophage numbers fluctuate during the second telogen, peaking during mid-telogen. They also showed that macrophage inhibition by clodronate liposomes during telogen was sufficient to induce anagen (Castellana et al., 2014). Our data support these findings genetically (with *Csf1r-CreER::R26-iDTR* mice), molecularly (with neutralizing antibodies), and pharmacologically (with Csf1r antagonists) (Figure 6). We also showed that knocking down OSM in cultured macrophages abrogates their ability to inhibit hair regeneration in a patch assay (Figures S3F–S3H). The importance of

(E) Flow cytometry for TREM2 in the telogen dermis. Macrophages (gated on CD45, F4/80, and CD11b) were further analyzed according to their TREM2 and MHC II expression. TREM2$^+$ macrophages tend to be MHC II^{low}, as expected, and their numbers decrease from early to late telogen (n = 999 during early telogen, falling to n = 88 by late telogen). Percentages calculated out of total dermal CD45$^+$ immune cells. Data are pooled from 2 biological replicates.
(F) Schematic diagram of telogen hair follicle with TREM2$^+$ macrophages that produce OSM, which signals via OSMRβ/gp130-JAK-STAT5 on HFSC to maintain stem cell quiescence.

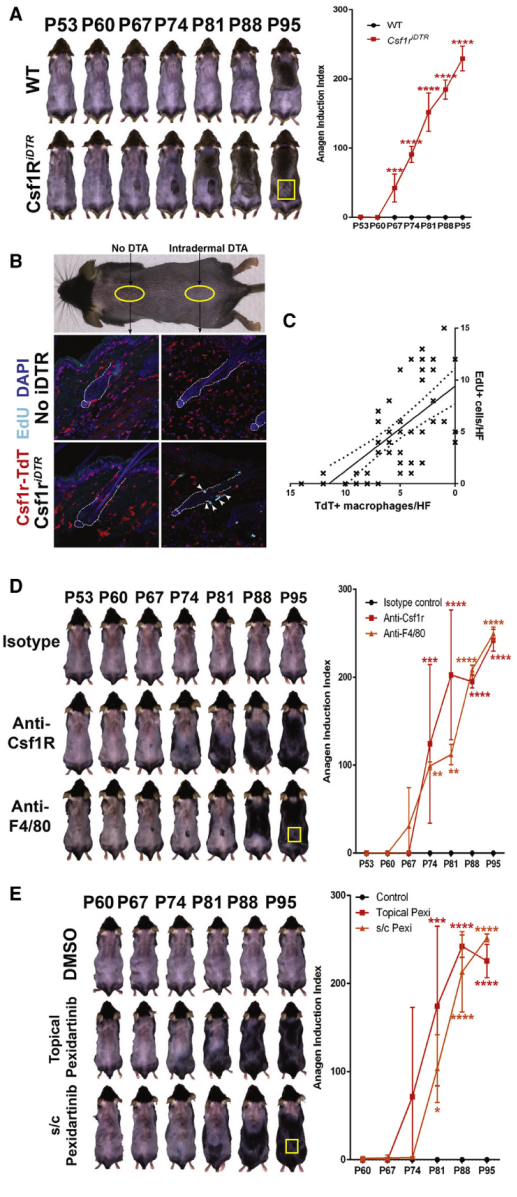

Figure 6. Macrophage Depletion or Inhibition during Telogen Initiates Anagen

(A) Genetic ablation of macrophages using *Csf1r-CreER::R26-iDTR* mice. Tamoxifen was administered systemically for 4 days from P53–P56, and 200 ng diphtheria toxin (DTA) (100 μL of 2 ng/μL DTA) was injected intradermally for 7 days from P60. A local anagen was initiated at the site of injection. Data are representative of 3 independent experiments, n = 2 mice per group.

(B and C) *Csf1r-CreER::R26-TdTomato::R26-iDTR* mice and littermate controls (no *R26-iDTR*) underwent tamoxifen induction and DTA administration as described in (A). Dermis from area of DTA injection, and a remote area on the dorsal skin, were collected and examined with IF and FACS. Intradermal DTA was associated with loss of perifollicular macrophages in *Csf1r-CreER::R26-iDTR* mice (B), which in turn was associated with increased proliferation of HFSCs highlighted by increased EdU incorporation (C). Data are representative of 2 independent experiments. (Quantification of 50 HFs in a 20× field across 2 mice. $R^2 = 0.4674$, $p < 0.0001$. Dotted lines represent 95% CI.)

(D) Neutralizing antibodies to Csf1r and F4/80 (500 μg/dose) injected intradermally into the middle of the dorsal skin of C57BL/6 mice for 14 days were sufficient to initiate a local anagen at the site of injection. Data are representative of 2 independent experiments, n = 3 mice per group.

(E) Pharmacological inhibition of Csf1r (5 day treatment) with the small molecule pexidartinib (1% in DMSO w/v) was similarly successful at initiating anagen when administered both topically and subcutaneously (s/c). Data are representative of 2 independent experiments, n = 3 mice per group.

Data are mean ± SEM. *$p < 0.05$, **$p < 0.01$, ***$p < 0.001$, ****$p < 0.0001$, in (A), (D), and (E) two-way ANOVA of various treatments at each time point.

trichophages in the maintenance of telogen reflects the emerging and diverse roles of macrophages across many tissues, including the brain, where they perform essential developmental and homeostatic functions like synaptic pruning (Nimmerjahn et al., 2005), and the heart where they facilitate electrical conduction (Hulsmans et al., 2017).

The genetic similarities between trichophages and microglia may offer some insights into the potential role of this cell type in the skin. Microglia are crucial supporting cells of the brain and CNS, where they carry out innate immune functions, clear cellular debris, and participate in homeostasis and pruning of neurons (Hanisch and Kettenmann, 2007). TREM2-DAP12 signaling in microglia has been functionally linked to their survival (Poliani et al., 2015) and plays a role in phagocytosis (Takahashi et al., 2007). Single-cell transcriptomics of mouse microglia has suggested that TREM2 is associated with phagocytic and homeostatic functions (Sousa et al., 2018). A subset of $TREM2^{hi}$ macrophages has also been identified in murine atherosclerotic plaques in which they play a non-immune, homeostatic role (Cochain et al., 2018). This function may be analogous to the role of $TREM2^{+}$ trichophages in the hair cycle, where they modulate HFSC activity and coordinate the cyclical growth and regression of hair follicles.

In humans, polymorphisms in TREM2 have been associated with both protection or progression of Alzheimer's disease (Ulrich et al., 2017), and $TREM2^{+}$ macrophages have also been detected in lesional biopsies of human artherosclerotic plaques (Cochain et al., 2018). Neutralizing antibodies to pathogenic TREM2 variants appear to prevent progressive of murine models of Alzheimer's disease (Cheng et al., 2018). Our work supports the role of TREM2 as a useful marker for a functionally distinct subset of macrophages, or, in our case, trichophages. Defining a role for TREM2 in these physiologic processes or other human pathologies, such as hair loss disorders, awaits further investigation.

While microglia are believed to be derived from the embryonic yolk sac (Ginhoux et al., 2010), and self-renew through life, the ontogeny of trichophages awaits further investigation. Dermal macrophages undergo constant replenishment from circulating monocytes (McGovern et al., 2014), likely reflecting the function

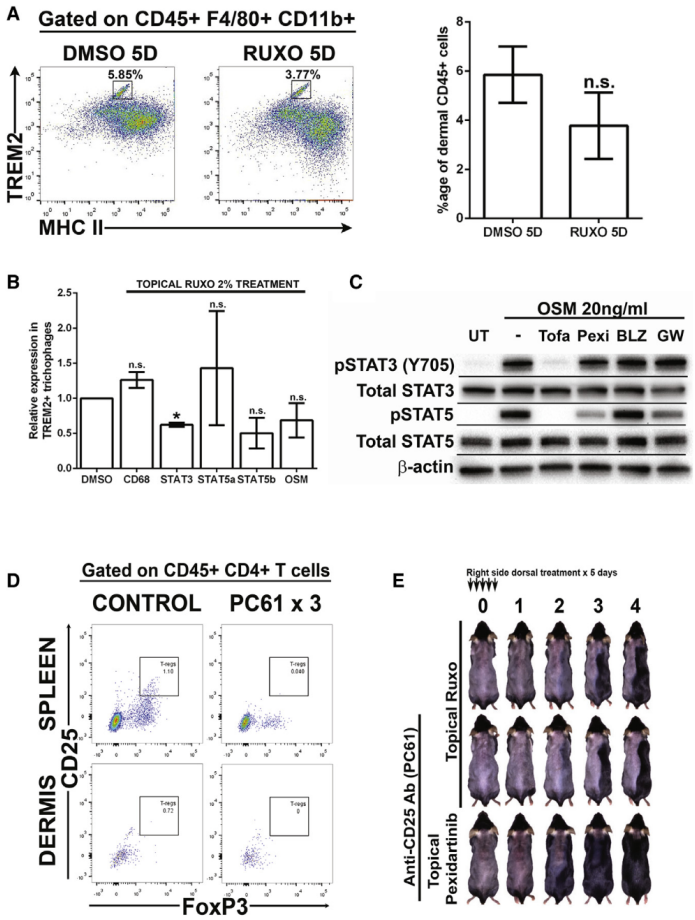

Figure 7. Csf1r Inhibitor Is Specific to Macrophages, and JAK Inhibition Is Specific to HFSCs

(A) FACS of dermis after 5-day treatment with topical DMSO or ruxolitinib 2% (w/v). Topical ruxolitinib treatment does not significantly reduce TREM2$^+$ macrophages in the dermis. Data are representative of n = 2 biological replicates.

(B) While treatment with topical ruxolitinib 2% significantly reduced STAT3 levels in TREM2$^+$ macrophages, it did not significantly levels of STAT5a, STAT5b or OSM. Data pool from n = 3 biological replicates.

(C) Treatment of cultured HFSCs with small-molecule inhibitors of Csf1r. Pexidartinib (Pexi), BLZ945 (BLZ), and GW2580 (GW) were all able to induce anagen in mouse telogen skin (Figure S7B). While there might be slight off-target pSTAT5 inhibition with Pexi and GW2580, BLZ945 had no effects on JAK-STAT signaling in HFSCs. This is reflected in the efficiency of anagen induction with these drugs (Pexi > GW > BLZ). Data are representative of 2 biological replicates.

(D) T regulatory cell (Treg) depletion with anti-CD25 neutralizing monoclonal antibody (PC61). C57BL/6 treated with 3 intraperitoneal injections of PC61 exhibited marked Treg depletion in the spleen and dermis. Data are representative of 2 independent experiments, with 2 mice per group.

(E) Mice treated with PC61 underwent JAK-inhibitor-initiated anagen with the same kinetics as WT mice. Likewise, mice treatment with the small molecule Csf1r tyrosine kinase inhibitor pexidartinib to target macrophages also underwent anagen initiation. Together, these data demonstrate that these processes are not dependent on Tregs. Data are representative of 2 independent experiments, n = 3 mice per group.

Data are mean ± SEM. *p < 0.05, **p < 0.01, ***p < 0.001, ****p < 0.0001. Student's t test.

of the skin as a barrier organ. In addition, while we have demonstrated that TREM2$^+$ trichophages are reduced in number just before spontaneous anagen, their precise fate thereafter is unknown. Whether trichophages undergo apoptosis, differentiate into another macrophage subset, or exit the skin entirely is an enticing question for future lineage tracing studies when specific TREM2 reporter tools become available.

In humans, OSM was first discovered as a negative growth regulator of the A375 melanoma cell line (Zarling et al., 1986), at a time when there was an increased interest in identifying endogenous negative regulators of cell growth (chalones) in the field of cancer research. While OSM was first isolated in the supernatant of histiocytic lymphoma cells (Zarling et al., 1986), it was found to be more reliably obtained from macrophage cell lines (Malik et al., 1989). Recently, OSM was also identified as a stem-cell niche maintenance factor in skeletal muscle via paracrine signaling (Sampath et al., 2018). Our findings suggest that OSM-producing macrophages interact with the murine HFSC niche, suggesting that this signaling axis may function in maintaining quiescence of other stem cell niches or perhaps cancer stem cells.

Murine HFSCs of the bulge and hair germ express both the receptor (OSMRβ) and co-receptor (gp130) necessary for OSM signaling, which occurs via the JAK-STAT and MAPK signaling pathways. We show here that STAT5 is the most likely downstream mediator of quiescence in HFSC, since the activated phosphorylated form of STAT5 in the HFSC coincides with the early-to-mid second telogen, and its genetic ablation was sufficient for initiating anagen during telogen. OSM signaling via the JAK-STAT5 pathway also inhibits adipocyte terminal differentiation (Miyaoka et al., 2006), delays cell-cycle entry in HepG2 cells (Klausen et al., 2000), and suppresses cytokine secretion in T cells (Hintzen et al., 2008b). Further, the murine OSMRβ subunit is believed to directly recruit JAK2 to phosphorylate STAT5 in response to ligand binding (Hintzen et al., 2008a). This positions the OSM-OSMRβ-JAK-STAT5

signaling axis as a conserved mechanism for maintaining cellular quiescence.

JAK-STAT3 signaling was previously shown to be required for the initiation of spontaneous anagen in mice, but not for plucking-induced anagen (Sano et al., 2000). We showed that both STAT3 and STAT5 are dynamically expressed across telogen, but that only pSTAT5 is specific for the HFSC during this phase. Further, using the covalent JAK3 inhibitor PF-06651600, we showed that inhibition of the JAK3-STAT5 signaling axis alone in HFSCs is sufficient to initiate anagen. The role of STAT3 in keratinocyte differentiation and migration therefore is distinct from the role of STAT5 in maintaining HFSC quiescence. STAT3 and STAT5 signaling likely contribute to complementary mechanisms of maintaining and proliferation and/or migration in HFSC and may interact in the coordination of the induced hair cycle (i.e., in response to plucking, depilation, and wounding).

In this study, both STAT5 and OSMRβ epidermal ablation resulted in a synchronous induction of hair growth across the dorsal skin of mice (Figures 2A and 2D), compared with the cranio-caudal wave normally seen during normal anagen, and consistent with a concurrent genetic ablation event across the entire skin. Epidermal STAT5 ablation had a much more striking hair induction phenotype when compared to epidermal OSMRβ ablation, suggesting that there may be other potential chalones that converge on STAT5 to maintain quiescence during telogen. This suggests a specific STAT5 inhibitor may be sufficient for promoting the telogen-to-anagen transition.

The maintenance of quiescence via JAK-STAT signaling is emerging as a common developmental theme, where its role is evolutionary conserved. JAK-STAT signaling in the *Drosophila* testis is mediated by the ligand *Unpaired*, which is the fly homolog of IL-6, and signals via STAT92E to prevent differentiation of the germline stem cells (Bausek, 2013). JAK2-STAT5 signaling in murine hepatic stellate stem cells mediates quiescence signals from vitamin A and insulin (Yoneda et al., 2016). In the murine mammary gland, another organ that undergoes controlled cycles of growth and involution, JAK-STAT3 transmits signals via LIF (another gp130-dependent cytokine) to mediate involution (Humphreys et al., 2002), while JAK-STAT5 transmits signals from prolactin during lactation to increase milk production (Hughes and Watson, 2012). Interestingly, during pregnancy and lactation, prolactin signaling occurs via JAK-STAT5 in the HFSC to maintain quiescence of the hair follicles, perhaps to conserve nutritional resources during pregnancy (Goldstein et al., 2014; Foitzik et al., 2003). Here, we show that the JAK-STAT5 pathway downstream of OSM is physiologically relevant during telogen in both male and female mice and may represent a paradigm in the control of stem cell quiescence.

Building on our previous observation that JAK inhibition of telogen skin was sufficient to induce hair growth, here we identified a OSM-OSMRβ-JAK-STAT5 signaling axis that maintains quiescence of HFSCs during telogen. We also identified the source of endogenous OSM as the trichophage, an immune cell that contributes to the quiescence of the HFSC niche during telogen. This finding reflects the current paradigm that attribute tissue homeostatic roles for immune cells in various tissues (Rankin and Artis, 2018). Future studies to determine whether OSM-producing trichophages exist in human skin and scalp will allow us to target this signaling axis to treat hair loss disorders associated with prolonged or arrested telogen, such as androgenetic alopecia. Therapeutic interventions aimed at specialized extra-follicular cell populations raises the intriguing possibility of treating human hair loss disorders by targeting a cell type outside the hair follicle itself.

STAR★METHODS

Detailed methods are provided in the online version of this paper and include the following:

- KEY RESOURCES TABLE
- CONTACT FOR REAGENT AND RESOURCE SHARING
- EXPERIMENTAL MODELS AND SUBJECT DETAILS
  - Animals
  - Tamoxifen Induction
  - EdU
- MATERIALS DETAILS
  - Hair Cycle Manipulation
  - Blocking and Neutralizing Antibodies
  - Flow Cytometry
  - Cell Culture
  - Quantitative Real-Time PCR
  - Western Blot
  - Immunofluorescence and Histology
  - shRNA
  - Macrophage Inhibition
  - Hair Reconstitution Assays
  - Single-cell RNA Sequencing
- QUANTIFICATION AND STATISTICAL ANALYSIS
  - Hair Cycle Analysis
  - Statistical Analysis
- DATA AVAILABILITY

SUPPLEMENTAL INFORMATION

Supplemental Information can be found online at https://doi.org/10.1016/j.stem.2019.01.011.

ACKNOWLEDGMENTS

We thank D. Owens, E. Ezratty, R. Clynes, and H. Snoeck for their valuable feedback and critical advice. We are also grateful for expert technical assistance from M. Zhang, E. Chang, J. Huang, W. Zeng, and D. Rong. E.C. Wang was funded by the National Skin Center of Singapore and the National Medical Research Council (NMRC) of Singapore. Research reported in this publication was performed in the CCTI Flow Cytometry Core, supported in part by NIH award S10OD020056. This work was supported in part by the Locks of Love Foundation and NIH/NIAMS grants P30 AR069632 (Epicure) and P50 AR070588 (AACORT).

AUTHOR CONTRIBUTIONS

E.C.E.W. designed the studies, performed the experiments, and analyzed the data. A.W.F. and C.G.D. designed and provided genetic models for the macrophage experiments. Z.D. performed additional experiments. A.M.C. oversaw all study design, interpretation of results, and data analysis. E.C.E.W. and A.M.C. wrote the manuscript.

DECLARATION OF INTERESTS

E.C.E.W., Z.D., and A.W.F. have no interests to declare. C.G.D. has served as a paid consultant for Agenus, Bayer, BMS, F-Star, Janssen, Merck, Pfizer, Pierre

Fabre, Roche/Genentech, and Shattuck Labs. He has ownership interest in Compugen, Harpoon, Kleo, Potenza, Tizona, and Werewolf. A.M.C. is a consultant and shareholder for Aclaris Therapeutics, Inc.; is a consultant for Dermira, Inc.; and has received grant funding from Pfizer, Inc. Columbia University has filed patents on the use of JAK inhibitors in the treatment of hair loss disorders.

Received: January 2, 2018
Revised: October 30, 2018
Accepted: January 26, 2019
Published: March 28, 2019

REFERENCES

Ali, N., Zirak, B., Rodriguez, R.S., Pauli, M.L., Truong, H.A., Lai, K., Ahn, R., Corbin, K., Lowe, M.M., Scharschmidt, T.C., et al. (2017). Regulatory T cells in skin facilitate epithelial stem cell differentiation. Cell *169*, 1119–1129.

Bausek, N. (2013). JAK-STAT signaling in stem cells and their niches in Drosophila. JAK-STAT *2*, e25686.

Castellana, D., Paus, R., and Perez-Moreno, M. (2014). Macrophages contribute to the cyclic activation of adult hair follicle stem cells. PLoS Biol. *12*, e1002002.

Cheng, Q., Danao, J., Talreja, S., Wen, P., Yin, J., Sun, N., Li, C.M., Chui, D., Tran, D., Koirala, S., et al. (2018). TREM2-activating antibodies abrogate the negative pleiotropic effects of the Alzheimer's disease variant *Trem2*^{R47H} on murine myeloid cell function. J. Biol. Chem. *293*, 12620–12633.

Cochain, C., Vafadarnejad, E., Arampatzi, P., Pelisek, J., Winkels, H., Ley, K., Wolf, D., Saliba, A.E., and Zernecke, A. (2018). Single-cell RNA-seq reveals the transcriptional landscape and heterogeneity of aortic macrophages in murine atherosclerosis. Circ. Res. *122*, 1661–1674.

Doles, J., Storer, M., Cozzuto, L., Roma, G., and Keyes, W.M. (2012). Age-associated inflammation inhibits epidermal stem cell function. Genes Dev. *26*, 2144–2153.

Eichmüller, S., van der Veen, C., Moll, I., Hermes, B., Hofmann, U., Müller-Röver, S., and Paus, R. (1998). Clusters of perifollicular macrophages in normal murine skin: Physiological degeneration of selected hair follicles by programmed organ deletion. J. Histochem. Cytochem. *46*, 361–370.

Flores, A., Schell, J., Krall, A.S., Jelinek, D., Miranda, M., Grigorian, M., Braas, D., White, A.C., Zhou, J.L., Graham, N.A., et al. (2017). Lactate dehydrogenase activity drives hair follicle stem cell activation. Nat. Cell Biol. *19*, 1017–1026.

Foitzik, K., Krause, K., Nixon, A.J., Ford, C.A., Ohnemus, U., Pearson, A.J., and Paus, R. (2003). Prolactin and its receptor are expressed in murine hair follicle epithelium, show hair cycle-dependent expression, and induce catagen. Am. J. Pathol. *162*, 1611–1621.

Ginhoux, F., Greter, M., Leboeuf, M., Nandi, S., See, P., Gokhan, S., Mehler, M.F., Conway, S.J., Ng, L.G., Stanley, E.R., et al. (2010). Fate mapping analysis reveals that adult microglia derive from primitive macrophages. Science *330*, 841–845.

Goldstein, J., Fletcher, S., Roth, E., Wu, C., Chun, A., and Horsley, V. (2014). Calcineurin/Nfatc1 signaling links skin stem cell quiescence to hormonal signaling during pregnancy and lactation. Genes Dev. *28*, 983–994.

Gómez-Lechón, M.J. (1999). Oncostatin M: Signal transduction and biological activity. Life Sci. *65*, 2019–2030.

Greco, V., Chen, T., Rendl, M., Schober, M., Pasolli, H.A., Stokes, N., Dela Cruz-Racelis, J., and Fuchs, E. (2009). A two-step mechanism for stem cell activation during hair regeneration. Cell Stem Cell *4*, 155–169.

Hanisch, U.K., and Kettenmann, H. (2007). Microglia: Active sensor and versatile effector cells in the normal and pathologic brain. Nat. Neurosci. *10*, 1387–1394.

Harel, S., Higgins, C.A., Cerise, J.E., Dai, Z., Chen, J.C., Clynes, R., and Christiano, A.M. (2015). Pharmacologic inhibition of JAK-STAT signaling promotes hair growth. Sci. Adv. *1*, e1500973.

Hintzen, C., Evers, C., Lippok, B.E., Volkmer, R., Heinrich, P.C., Radtke, S., and Hermanns, H.M. (2008a). Box 2 region of the oncostatin M receptor determines specificity for recruitment of Janus kinases and STAT5 activation. J. Biol. Chem. *283*, 19465–19477.

Hintzen, C., Haan, C., Tuckermann, J.P., Heinrich, P.C., and Hermanns, H.M. (2008b). Oncostatin M-induced and constitutive activation of the JAK2/STAT5/CIS pathway suppresses CCL1, but not CCL7 and CCL8, chemokine expression. J. Immunol. *181*, 7341–7349.

Hsu, Y.C., Pasolli, H.A., and Fuchs, E. (2011). Dynamicss between stem cells, niche, and progeny in the hair follicle. Cell *144*, 92–105.

Hughes, K., and Watson, C.J. (2012). The spectrum of STAT functions in mammary gland development. JAK-STAT *1*, 151–158.

Hulsmans, M., Clauss, S., Xiao, L., Aguirre, A.D., King, K.R., Hanley, A., Hucker, W.J., Wulfers, E.M., Seemann, G., Courties, G., et al. (2017). Macrophages facilitate electrical conduction in the heart. Cell *169*, 510–522.

Humphreys, R.C., Bierie, B., Zhao, L., Raz, R., Levy, D., and Hennighausen, L. (2002). Deletion of Stat3 blocks mammary gland involution and extends functional competence of the secretory epithelium in the absence of lactogenic stimuli. Endocrinology *143*, 3641–3650.

Iversen, O.H. (1981). The Chalones. In Tissue Growth Factors, R. Baserga, ed. (Springer).

Klausen, P., Pedersen, L., Jurlander, J., and Baumann, H. (2000). Oncostatin M and interleukin 6 inhibit cell cycle progression by prevention of p27kip1 degradation in HepG2 cells. Oncogene *19*, 3675–3683.

Kwack, M.H., Ahn, J.S., Kim, M.K., Kim, J.C., and Sung, Y.K. (2012). Dihydrotestosterone-inducible IL-6 inhibits elongation of human hair shafts by suppressing matrix cell proliferation and promotes regression of hair follicles in mice. J. Invest. Dermatol. *132*, 43–49.

MacDonald, K.P., Palmer, J.S., Cronau, S., Seppanen, E., Olver, S., Raffelt, N.C., Kuns, R., Pettit, A.R., Clouston, A., Wainwright, B., et al. (2010). An antibody against the colony-stimulating factor 1 receptor depletes the resident subset of monocytes and tissue- and tumor-associated macrophages but does not inhibit inflammation. Blood *116*, 3955–3963.

Malik, N., Kallestad, J.C., Gunderson, N.L., Austin, S.D., Neubauer, M.G., Ochs, V., Marquardt, H., Zarling, J.M., Shoyab, M., Wei, C.M., et al. (1989). Molecular cloning, sequence analysis, and functional expression of a novel growth regulator, oncostatin M. Mol. Cell. Biol. *9*, 2847–2853.

Martinez-Pomares, L., Platt, N., McKnight, A.J., da Silva, R.P., and Gordon, S. (1996). Macrophage membrane molecules: Markers of tissue differentiation and heterogeneity. Immunobiology *195*, 407–416.

McGovern, N., Schlitzer, A., Gunawan, M., Jardine, L., Shin, A., Poyner, E., Green, K., Dickinson, R., Wang, X.N., Low, D., et al. (2014). Human dermal CD14^{+} cells are a transient population of monocyte-derived macrophages. Immunity *41*, 465–477.

Miyaoka, Y., Tanaka, M., Naiki, T., and Miyajima, A. (2006). Oncostatin M inhibits adipogenesis through the RAS/ERK and STAT5 signaling pathways. J. Biol. Chem. *281*, 37913–37920.

Müller-Newen, G. (2003). The cytokine receptor gp130: Faithfully promiscuous. Sci. STKE *2003*, PE40.

Müller-Röver, S., Handjiski, B., van der Veen, C., Eichmüller, S., Foitzik, K., McKay, I.A., Stenn, K.S., and Paus, R. (2001). A comprehensive guide for the accurate classification of murine hair follicles in distinct hair cycle stages. J. Invest. Dermatol. *117*, 3–15.

Nimmerjahn, A., Kirchhoff, F., and Helmchen, F. (2005). Resting microglial cells are highly dynamic surveillants of brain parenchyma in vivo. Science *308*, 1314–1318.

Paus, R., Stenn, K.S., and Link, R.E. (1990). Telogen skin contains an inhibitor of hair growth. Br. J. Dermatol. *122*, 777–784.

Paus, R., van der Veen, C., Eichmüller, S., Kopp, T., Hagen, E., Müller-Röver, S., and Hofmann, U. (1998). Generation and cyclic remodeling of the hair follicle immune system in mice. J. Invest. Dermatol. *111*, 7–18.

Plikus, M.V., Mayer, J.A., de la Cruz, D., Baker, R.E., Maini, P.K., Maxson, R., and Chuong, C.M. (2008). Cyclic dermal BMP signalling regulates stem cell activation during hair regeneration. Nature *451*, 340–344.

Poliani, P.L., Wang, Y., Fontana, E., Robinette, M.L., Yamanishi, Y., Gilfillan, S., and Colonna, M. (2015). TREM2 sustains microglial expansion during aging and response to demyelination. J. Clin. Invest. *125*, 2161–2170.

Rankin, L.C., and Artis, D. (2018). Beyond host defense: Emerging functions of the immune system in regulating complex tissue physiology. Cell *173*, 554–567.

Rezza, A., Wang, Z., Sennett, R., Qiao, W., Wang, D., Heitman, N., Mok, K.W., Clavel, C., Yi, R., Zandstra, P., et al. (2016). Signaling networks among stem cell precursors, transit-amplifying progenitors, and their niche in developing hair follicles. Cell Rep. *14*, 3001–3018.

Rose, T.M., and Bruce, A.G. (1991). Oncostatin M is a member of a cytokine family that includes leukemia-inhibitory factor, granulocyte colony-stimulating factor, and interleukin 6. Proc. Natl. Acad. Sci. USA *88*, 8641–8645.

Rose-John, S. (2018). Interleukin-6 family cytokines. Cold Spring Harb. Perspect. Biol. *10*. Published online February 1, 2018. https://doi.org/10.1101/cshperspect.a028415.

Sampath, S.C., Sampath, S.C., Ho, A.T.V., Corbel, S.Y., Millstone, J.D., Lamb, J., Walker, J., Kinzel, B., Schmedt, C., and Blau, H.M. (2018). Induction of muscle stem cell quiescence by the secreted niche factor Oncostatin M. Nat. Commun. *9*, 1531.

Sano, S., Kira, M., Takagi, S., Yoshikawa, K., Takeda, J., and Itami, S. (2000). Two distinct signaling pathways in hair cycle induction: Stat3-dependent and -independent pathways. Proc. Natl. Acad. Sci. USA *97*, 13824–13829.

Sasmono, R.T., Oceandy, D., Pollard, J.W., Tong, W., Pavli, P., Wainwright, B.J., Ostrowski, M.C., Himes, S.R., and Hume, D.A. (2003). A macrophage colony-stimulating factor receptor-green fluorescent protein transgene is expressed throughout the mononuclear phagocyte system of the mouse. Blood *101*, 1155–1163.

Segawa, M., Fukada, S., Yamamoto, Y., Yahagi, H., Kanematsu, M., Sato, M., Ito, T., Uezumi, A., Hayashi, S., Miyagoe-Suzuki, Y., et al. (2008). Suppression of macrophage functions impairs skeletal muscle regeneration with severe fibrosis. Exp. Cell Res. *314*, 3232–3244.

Sennett, R., Wang, Z., Rezza, A., Grisanti, L., Roitershtein, N., Sicchio, C., Mok, K.W., Heitman, N.J., Clavel, C., Ma'ayan, A., and Rendl, M. (2015). An integrated transcriptome atlas of embryonic hair follicle progenitors, their niche, and the developing skin. Dev. Cell *34*, 577–591.

Sousa, C., Golebiewska, A., Poovathingal, S.K., Kaoma, T., Pires-Afonso, Y., Martina, S., Coowar, D., Azuaje, F., Skupin, A., Balling, R., et al. (2018). Single-cell transcriptomics reveals distinct inflammation-induced microglia signatures. EMBO Rep. *19*, e46171.

Stenn, K.S., and Paus, R. (2001). Controls of hair follicle cycling. Physiol. Rev. *81*, 449–494.

Suzuki, S., Kato, T., Takimoto, H., Masui, S., Oshima, H., Ozawa, K., Suzuki, S., and Imamura, T. (1998). Localization of rat FGF-5 protein in skin macrophage-like cells and FGF-5S protein in hair follicle: Possible involvement of two Fgf-5 gene products in hair growth cycle regulation. J. Invest. Dermatol. *111*, 963–972.

Suzuki, S., Ota, Y., Ozawa, K., and Imamura, T. (2000). Dual-mode regulation of hair growth cycle by two Fgf-5 gene products. J. Invest. Dermatol. *114*, 456–463.

Takahashi, K., Prinz, M., Stagi, M., Chechneva, O., and Neumann, H. (2007). TREM2-transduced myeloid precursors mediate nervous tissue debris clearance and facilitate recovery in an animal model of multiple sclerosis. PLoS Med. *4*, e124.

Ulrich, J.D., Ulland, T.K., Colonna, M., and Holtzman, D.M. (2017). Elucidating the Role of TREM2 in Alzheimer's Disease. Neuron *94*, 237–248.

Weisser, S.B., McLarren, K.W., Kuroda, E., and Sly, L.M. (2013). Generation and characterization of murine alternatively activated macrophages. Methods Mol. Biol. *946*, 225–239.

Yoneda, A., Sakai-Sawada, K., Niitsu, Y., and Tamura, Y. (2016). Vitamin A and insulin are required for the maintenance of hepatic stellate cell quiescence. Exp. Cell Res. *341*, 8–17.

Yu, M., Kissling, S., Freyschmidt-Paul, P., Hoffmann, R., Shapiro, J., and McElwee, K.J. (2008). Interleukin-6 cytokine family member oncostatin M is a hair-follicle-expressed factor with hair growth inhibitory properties. Exp. Dermatol. *17*, 12–19.

Zarling, J.M., Shoyab, M., Marquardt, H., Hanson, M.B., Lioubin, M.N., and Todaro, G.J. (1986). Oncostatin M: A growth regulator produced by differentiated histiocytic lymphoma cells. Proc. Natl. Acad. Sci. USA *83*, 9739–9743.

STAR★METHODS

KEY RESOURCES TABLE

REAGENT or RESOURCE	SOURCE	IDENTIFIER
Antibodies		
Anti-Mouse OSMRβ	R&D Systems	Cat# MAB662; RRID:AB_2156568
Anti-Mouse pSTAT1 (Y701) (58D6)	Cell Signaling	Cat# 9167; RRID:AB_561284
Anti-Mouse pSTAT3 (Y705) (D3A7)	Cell Signaling	Cat# 9145; RRID:AB_2491009
Anti-Mouse pSTAT3 (S727)	Abcam	Cat# ab86430; RRID:AB_10713219
Anti-Mouse total STAT3 (D3Z2G)	Cell Signaling	Cat# 12640; RRID:AB_2629499
Anti-Mouse pSTAT5 (Y694) (C11C5)	Cell Signaling	Cat# 9359; RRID:AB_823649
Anti-Mouse total STAT5 (3H7)	Cell Signaling	Cat# 9358; RRID:AB_659905
Anti-Mouse pMEK-1/2 (Ser217/221) (41G9)	Cell Signaling	Cat# 9154; RRID:AB_2138017
Anti-Mouse pERK-1/2 (Thr202/Tyr204) (197G2)	Cell Signaling	Cat# 4377; RRID:AB_331775
Anti-Mouse pAkt (Thr308) (C31E5E)	Cell Signaling	Cat# 2965; RRID:AB_2255933
Anti-Mouse mTOR (7C10)	Cell Signaling	Cat# 2983; RRID:AB_2105622
Anti-Mouse pJAK1 (Tyr1022/1023)	Cell Signaling	Cat# 3331; RRID:AB_2265057
Anti-Mouse pJAK2 (D4A8)	Cell Signaling	Cat# 8082; RRID:AB_10949104
Anti-Mouse pJAK3 (D44E3)	Cell Signaling	Cat# 5031; RRID:AB_10612243
Anti-Mouse pTyk2 (D7T8A)	Cell Signaling	Cat# 68790
Anti-Mouse β-actin-HRP	Santa Cruz	Cat# sc-47778; RRID:AB_2714189
Anti-Mouse GAPDH (6C5)	Santa Cruz	Cat# sc-32233; RRID:AB_627679
Anti-Mouse ITGA6 FITC	Serotec	Cat# MCA699F; RRID:AB_324269
Anti-Mouse CD34 A700	eBioscience	Cat# 56-0341-82; RRID:AB_493998
Anti-Mouse Sca-1 APC	eBioscience	Cat# 17-5981-81; RRID:AB_469486
Anti-Mouse P-cadherin PE	R&D Systems	Cat# FAB761P; RRID:AB_2291533
Anti-Mouse P-cadherin	R&D Systems	Cat# AF761; RRID:AB_355581
Anti-Mouse gp130	Neuromics	Cat# MO15024; RRID:AB_1610306
Anti-Mouse/Human Keratin 15	Covance	Cat# PCK-153P-100; RRID:AB_291540
Anti-Mouse CD34	eBioscience	Cat# 14-0341-82; RRID:AB_467210
Anti-Mouse CD45 FITC	Biolegend	Cat# 103108; RRID:AB_312973
Anti-Mouse CD45 Alexa 700	BD PharMingen	Cat# 560510; RRID:AB_1645208
Anti-Mouse CD3 PE-eFluor 610	Thermo Fisher Scientific	Cat# 61-0031-82; RRID:AB_2574514
Anti-Mouse CD19 PE-eFluor 610	Thermo Fisher Scientific	Cat# 61-0193-82; RRID:AB_2574536
Anti-Mouse NK1.1 PE-eFluor 610	Thermo Fisher Scientific	Cat# 61-5941-80; RRID:AB_2574641
Anti-Mouse Integrin-α9 PE	R&D Systems	Cat# FAB3827P; RRID:AB_10971625
Anti-Mouse F4/80 PE-Cy7	BioLegend	Cat# 123114; RRID:AB_893478
Anti-Mouse F4/80 Percp-cy5.5	Biolegend	Cat# 123126; RRID:AB_893483
Anti-Mouse CD11b APC	BD PharMingen	Cat# 557686; RRID:AB_396796
Anti-Mouse CD11b PE	eBioscience	Cat# 12-0112-81; RRID:AB_465546
Anti-Mouse CD11b APC-eFluor 780	Thermo Fisher Scientific	Cat# 47-0112-82; RRID:AB_1603193
Anti-Mouse CD11b FITC	Biolegend	Cat# 101205; RRID:AB_312788
Anti-Mouse CD11c BV605	Biolegend	Cat# 117334; RRID:AB_2562415
Anti-Mouse Ly6G BV650	Biolegend	Cat# 127641; RRID:AB_2565881
Anti-Mouse CD163 FITC	BioRAD	Cat# MCA342F; RRID:AB_321967
Anti-Mouse CD206 APC	eBioscience	Cat# 17-2061-82; RRID:AB_2637420
Anti-Mouse I-A/I-E APC	Biolegend	Cat# 107617; RRID:AB_493526
Anti-Mouse I-A/I-E V500	BD PharMingen	Cat# 562366; RRID:AB_11153488
Anti-Mouse OSM	Abcam	Cat# ab133748

(*Continued on next page*)

Continued

REAGENT or RESOURCE	SOURCE	IDENTIFIER
Anti-Mouse CD11b	Abcam	Cat# ab8878; RRID:AB_306831
Anti-Mouse Aif-1/Iba-1	Novus Biologicals	Cat#NB100-1028; RRID:AB_521594
Anti-Mouse F4/80	Life Technologies	Cat# 14-4801-82; RRID:AB_467558
Anti-Mouse Trem2	Abcam	Cat# ab95470; RRID:AB_10679173
Anti-Mouse Trem2-APC	R&D Systems	Cat# FAB17291A; RRID:AB_884527
InVivoMAb Anti-Mouse Csf1R (CD115)	BioXCell	Cat# AFS98; RRID:AB_2687699
InVivoMAb Anti-mouse F4/80 (CI:A3-1)	BioXCell	Cat# BE0206; RRID:AB_10949019
InVivoPlus Anti-mouse CD25 (IL-2Rα) (PC-61.5.3)	BioXCell	Cat# BP0012; RRID:AB_1107619
InVivoPlus Mouse IgG2 isotype control	BioXCell	Cat# BP0086; RRID:AB_1107791
Bacterial and Virus Strains		
pLKO.1 - TRC cloning vector	Addgene	Cat# 10878; RRID:Addgene_10878
pMD2.G – packaging plasmid	Addgene	Cat# 12259; RRID:Addgene_12259
pCMV delta R8.2 – packaging plasmid	Addgene	Cat# 12263; RRID:Addgene_12263
Chemicals, Peptides, and Recombinant Proteins		
DMSO	Sigma-Aldrich	Cat# D2650-100ML
Ruxolitinib	APExBIO	Cat# INCB018424
Tofacinitb	Abmole Bioscience	Cat# CP-690550
PF-06651600	Sigma	Cat# PZ0316-25MG
Recombinant Murine OSM	R&D Systems	Cat# 495-MO-025
Trypsin 2.5%	Fisher Scientific	Cat# 15090046
Collagenase IV from Clostridium histolyticum	Sigma-Aldrich	Cat# C5138
DNase I	Sigma-Aldrich	Cat# D5025
CnT-07S Keratinocyte media	CELLnTEC	Cat# CnT-07
Diphtheria Toxin from Corynebacterium diphtheriae	Sigma-Aldrich	Cat# D0564
Tamoxifen	Sigma-Aldrich	Cat# T5648-1G
EdU (5-ethynyl-2′-deoxyuridine)	Life Technologies	Cat# A10044
DAPI	BioLegend	Cat# 422801
Pexidartinib	Selleckchem	Cat# S7818
BLZ945	Selleckchem	Cat# S7725
GW2580	Selleckchem	Cat# S8042
Telatinib	Selleckchem	Cat# S2231
Recombinant Murine M-CSF	Peprotech	Cat# 315-02
Lipofectamine 3000 Transfection Reagent	Thermo Fisher	Cat# L3000008
PEG-it viral precipitant	System Biosciences	Cat# LV810A-1
Critical Commercial Assays		
Click-iT Plus EdU Alexa Fluor 647 Imaging Kit	ThermoFisher	Cat# C10640
RNeasy Micro Kit	QIAgen	Cat# 74004
RNAscope	Advanced Cell Diagnostics	Cat# 320850
Experimental Models: Organisms/Strains		
Mouse: C57BL/6J	The Jackson Laboratory	JAX: 000664; RRID:IMSR_JAX:000664
Mouse: B6N.129S6(Cg)-Krt5$^{tm1.1(cre/ERT2)Blh}$/J	The Jackson Laboratory	JAX: 029155; RRID:IMSR_JAX:029155
Mouse: B6;129-Osmr$^{tm1.1Nat}$/J	The Jackson Laboratory	JAX: 011081; RRID:IMSR_JAX:011081
Mouse: B6.129S6-Stat5b^{tm1Mam} Stat5a^{tm2Mam}/Mmjax	The Jackson Laboratory	JAX: 32053-JAX
Mouse: FVB-Tg(Csf1r-cre/Esr1*)1Jwp/J	The Jackson Laboratory	JAX: 019098; RRID:IMSR_JAX:019098
Mouse: C57BL/6-Gt(ROSA)26Sor$^{tm1(HBEGF)Awai}$/J	The Jackson Laboratory	JAX: 007900; RRID:IMSR_JAX:007900
Mouse: C57BL/6-Tg(Foxp3-DTR/EGFP)23.2Spar/Mmjax	The Jackson Laboratory	JAX: 32050-JAX
Mouse: B6(SJL)-Foxn1nu-2J/GrsrJ	The Jackson Laboratory	JAX: 016195; RRID:IMSR_JAX:016195

(*Continued on next page*)

Continued

REAGENT or RESOURCE	SOURCE	IDENTIFIER
Oligonucleotides		
Osmr F	TCT GGG TGG AGA ATT ATA GC	N/A
Osmr R	CCA GGA ACT CCA GTT GCC CC	N/A
Osm F	ATG CAG ACA CGG CTT CTA AGA	N/A
Osm R	TTG GAG CAG CCA CGA TTG G	N/A
STAT5a F	CGC CAG ATG CAA GTG TTG TAT	N/A
STAT5a R	TCC TGG GGA TTA TCC AAG TCA AT	N/A
STAT5b F	CAC AGT GGA TCG AAA GCC AAG	N/A
STAT5b R	AGC TGG GTG GCC TTA ATG TTC	N/A
Keratin 17 F	ACC ATC CGC CAG TTT ACC TC	N/A
Keratin 17 R	CTA CCC AGG CCA CTA GCT GA	N/A
Il6st (gp130) F	GGT CAA CTT TTG GAA CCG TG	N/A
Il6st (gp130) R	GCA GCA TGG TTG GTC TTC C	N/A
Osm shRNA F	CGG CAC AAT ATC CTC GGC ATA	N/A
Osm shRNA R	TAT GCC GAG GAT ATT GTG CCG	N/A
GAPDH F	TGG CCT TCC GTG TTC CTA C	N/A
GAPDH R	GAG TTG CTG TTG AAG TCG CA	N/A
Software and Algorithms		
Graphpad Prism	Graphpad Software, Inc	https://www.graphpad.com/
FlowJo	FlowJo, LLC	https://www.flowjo.com/solutions/flowjo
ImageJ	MIH Version	https://imagej.nih.gov/ij/download.html
Loupe Cell Browser	10X Genomics	https://support.10xgenomics.com/single-cell-gene-expression/software/downloads/latest
Seurat	R Package	https://satijalab.org/seurat/
Deposited Data		
Single-cell RNA sequencing data	This study	GEO: GSE108709

CONTACT FOR REAGENT AND RESOURCE SHARING

Further information and requests for resources and reagents should be directed to and will be fulfilled by the Lead Contact, Angela Christiano (amc65@columbia.edu).

EXPERIMENTAL MODELS AND SUBJECT DETAILS

Animals

Mice were bred and maintained in the Russ Berrie Medical Sciences Pavilion Animal Facility in accordance with guidelines of the Institute of Comparative Medicine (ICM) and Institutional Animal Care and Use Committee (IACUC) of Columbia University. The Facility is specific pathogen-free, and all mice were socially housed under a 12 hour light/dark cycle. All mice were bred in the facility so as to have documented birth dates for accurate ages. All experiments were performed during the early- to mid-telogen phase of the hair cycle, or at the end of the previous anagen phase (P35 – P60), unless otherwise specified. *K5-CreERT$_2$::OSMRβ$^{FL/FL}$* or *K5-CreERT$_2$::STAT5a/b$^{FL/FL}$* were compared with control littermates (No CreER or *OSMRβ$^{wt/wt}$/STAT5a/b$^{wt/wt}$*). *Csf1r-CreER* mice (originally FVB) were backcrossed at least 6-9 generations into a C57BL/6 background. For genetic ablation of macrophages, *Csf1r-CreER::R26-iDTR* mice were compared with control WT littermates (no CreER or no *R26-iDTR*) after DTA administration (200ng per intradermal or intraperitoneal dose). *Csf1r-CreER* mice were provided by Dr. Anthony W. Ferrante, and *R26-iDTR* mice were provided by Dr. David Owens. Experiments were performed on both male and female mice where specified, and only in male mice when this distinction is not highlighted in the legend.

Tamoxifen Induction

Tamoxifen (Sigma-Aldrich) was dissolved in corn oil to a concentration of 10mg/ml, and mice were injected intraperitoneally (200μl) under light-protected conditions for 4 consecutive days during mid-telogen or otherwise stated.

EdU

5-ethnyl-2′-deoxyuridine (EdU, Life Technologies) was dissolved in sterile PBS to a concentration of 10mg/ml. For cellular dynamic studies, a single dose of 50μg/g was injected intraperitoneally 24 hours prior to sacrifice.

MATERIALS DETAILS

Hair Cycle Manipulation

Mice were carefully shaved with clippers during telogen to reveal the pink skin typical of the telogen phase 1 week prior to the experiment. Mice that were inadvertently wounded were not used. Anagen was induced by topical application of 2% Ruxolitinib in DMSO to the right side of the dorsal skin daily for 5 consecutive days starting at P60 (60^{th} post-natal day, mid-telogen). The hair cycle was observed and documented with standardized photographs taken prior to the first treatment, and then twice weekly thereafter. Murine IL-6, LIF or OSM (100ng/ml, 50ng/ml, 125ng/ml respectively) were dissolved in sterile PBS and 100μl was injected into the center of the field of application daily for 10 consecutive days, beginning with the first application of Ruxolitinib.

Blocking and Neutralizing Antibodies

For *in vitro* experiments, blocking antibodies were reconstituted at a concentration of 0.5mg/ml and diluted in keratinocyte media in 1:20, 1:100 and 1:1000 dilutions. Cultured cells were incubated with antibodies for 1 hour before addition of OSM. For *in vivo* experiments, antibodies to OSMR (7.5μg) were injected intradermally into the dorsal telogen skin daily for 14 days from P60 (mid-telogen). Neutralizing antibodies to Csf1r (AFS98) and F4/80 (CI:A3-1) were diluted in sterile PBS, and 500μg was injected intradermally into the dorsal telogen skin for 14 consecutive days. Neutralizing antibodies to CD25 (PC61.5) were injected intraperitoneally every other day (250μg/dose x 3) from P53, prior to anagen induction at P60.

Flow Cytometry

Dorsal skin was processed for either epidermal or dermal single-cell suspensions for stem cell or immune cell analysis by flow cytometry. Full thickness skin was harvested and defatted, and floated on 0.25% Trypsin for 30 min at 37°C. Epidermal cells were scraped off and titurated in DMEM/10%FBS before filtering through a 70μm mesh and centrifuged to obtain the epidermal cell pellet. The dermis was macerated finely with dissection scissors and re-suspended in 5ml DMEM with 0.2% Collagenase IV and 300U DNase 1, and incubated in a 37°C water bath for 40 minutes. The digested dermis was titurated in DMEM/10%FBS and filtered through a 70μm mesh and centrifuged. Cells were labeled with conjugated surface antibodies listed in the Key Resources Table in DMEM/2%FBS for 1h on ice, and washed and labeled with DAPI prior to FACS. Flow cytometry was performed on the Influx sorter in the Columbia University Flow Cytometry Core. Epidermal cell suspensions were used for HFSC stem cell analysis, and dermal suspensions were sorted for DP and immune cell experiments. Cells were collected in DMEM/10%FBS for cell culture, or in Trizol for RNA extraction. Flow cytometry data was analyzed using FlowJo software (FlowJo, LLC).

Cell Culture

HFSCs (ITGA6+ Sca-1-) cells were collected from flow cytometry and plated onto 6-well plates, and maintained with Cnt-07S keratinocyte media. *In vitro* stimulation experiments were carried out when keratinocytes were 80%–90% confluent. Confluent HFSCs were pre-treated with JAK inhibitors (tofacitinib, ruxolitinib or PF-06651600, all at 10μM – this high dose was chosen for complete JAK inhibition for this short experiment) for 20 min, and recombinant murine OSM was added for a final concentration of 10ng/ml or 20ng/ml for 15 min. For clonogenic assays, HFSCs were plated at a density of 10,000 cells per well and maintained for 2 weeks. Tofacitinib concentration for clonogenic assays was 100nM, based on the effects reported on mouse keratinocytes by Doles et al. (2012). For analysis of clonogenicity, plates were washed with PBS, and keratinocytes were fixed *in situ* with 4% paraformaldehyde (PFA) for 1 hour, followed by staining with 1% (wt/vol) Rhodamine B (Sigma-Aldrich) for 1h. Clones were quantified using a backlight.

Quantitative Real-Time PCR

Sorted cell populations, epidermal sheets or dermal tissue was collected in Trizol and flash-frozen overnight at −80°C. RNA was extracted with the QIAgen RNeasy Micro Kit and cDNA was made using Superscript IV with a 2:1 mixture of random hexamers and oligo-dT primers. Semiquantitative PCR for genes listed in the Key Resources Table was performed using SYBR Green PCR mix on an Applied Biosystems 7300 Real-Time PCR System. Primers for GAPDH were used in each reaction as a housekeeping control, and fold changes were calculated using the δ-δ Ct algorithm.

Western Blot

Cells were lyzed in RIPA buffer in the presence of protease and phosphatase inhibitors on ice, and protein lysates were resuspended in Laemmli sample buffer. Whole-cell lysates were fractionated on TGX Stain-free protein gels and transferred to a PVDF membrane, blocked with 5% non-fat milk in TBST, and incubated with antibodies listed in the Key Resources Table (all 1:1000, diluted in TBST/3%BSA) overnight. Membranes were washed the following day and incubated with HRP-conjugated secondary antibodies (1:5000), washed, and developed with Luminata Forte Western HRP Substrate and visualized on the BioRAD ChemiDOC MP Imaging system. GAPDH or β-actin were used as loading controls, depending on the mass of the proteins of interest.

Immunofluorescence and Histology

For immunofluorescence (IF) studies, dorsal skin or human scalp biopsies were submerged in 4% PFA for 1 hour, washed in PBS, and allowed to sink in 30% sucrose overnight before being embedded and frozen in OCT over liquid nitrogen. Samples were sectioned at 8μm thickness (unless otherwise specified) onto SuperFrost Plus glass slides (Fisher Scientific), blocked with 2% fish skin gelatin in PBS/0.3%Triton-X, and labeled with primary antibodies listed in Key Resources Table overnight at 4°C. Primary antibodies were washed off the following day, and labeled with fluorescence-conjugated secondary antibodies (1:1000), and images were acquired on a Zeiss LSM 5 Exciter Confocal microscope. EdU labeling was carried out with Click-iT Plus Alexa Fluor 647nm Imaging Kit according to manufacturer's protocol. For histology, formalin-fixed paraffin-embedded (FFPE) sections of mouse dorsal skin were rehydrated in increasingly dilute ethanol concentrations, and stained with hematoxylin and eosin.

shRNA

Hairpin sequences containing scramble or OSM 21mers obtained from the TRC RNAi consortium were cloned into the pLKO.1 library vector between the AgeI and EcoRI restriction sites. Modified pLKO.1 vector, along with helper packaging plasmids pMD2.G and pCMVδR8.2, were transfected into 293FT cells in the presence of Lipofectamine 3000 reagent, used according to manufacturer's protocol. Supernatant containing lentivirus was harvested 48 hours after transfection, filtered through a 0.45μm syringe filter, concentrated with PEG-it viral precipitant, resuspended in sterile PBS, and stored at −80°C until required.

Macrophage Inhibition

For *in vivo* macrophage inhibition, the small molecule pexidartinib/PLX3397 was administered topically (1% in DMSO wt/vol) or subcutaneously (1mM in corn oil) for 5 consecutive days from P60. Topical BLZ945, GW2580 and Telatinib were all also used at 1% in DMSO (wt/vol) and treated to the right dorsal back skin for 5 consecutive days. For OSM knock-down, peritoneal macrophages were harvested from adult C57BL/6 mice and cultured in DMEM/F12/15%FBS/0.3mMCa^{2+} the presence of 0.1mg/ml M-CSF to polarize them to an "M2-like" phenotype. Lentiviral precipitate containing scrambled or OSM shRNA added to the media in the presence of 8μg/ml protamine sulfate, and the cells were centrifuged at 3000rpm for 1h at 32°C to enhance transduction. Successful transductions were enriched with puromycin (1μg/ml) selection, counted and used for the patch assay.

Hair Reconstitution Assays

Neonatal (P0 or P1) mice were sacrificed and skins were harvested for the patch assay. Neonatal skins were enzymatically separated with 0.25% trypsin, and the dermis was further digested with 0.3% collagenase/DNase. Neonatal keratinocytes and dermal cells were counted recombined in a 1:1 ratio (10^6 cells each) and resuspended in 100μl of media (1:1 mix of DMEM/10%FBS and CnT-0.7S) and injected intradermally into the dorsal skin of a *nude* mouse. For pharmacological/cytokine treatment, tofacitinib (400nM) and/or OSM (25ng/ml) was added. For macrophage inhibition assays, 20×10^3 macrophages (either freshly sorted by FACS, or cultured) were added to the cell slurry before subcutaneous injection into the *Foxn1*$^{nu\text{-}2J}$ *nude* mouse. The patch assay was analyzed 2 weeks after injection, whereby subcutaneous cysts would have formed. Cysts, some containing hair fibers and follicles, were photographed, then digested with 0.35% collagenase IV in a 37°C waterbath overnight. Hair fibers and follicles were collected and counted manually under a dissection stereo microscope.

Single-cell RNA Sequencing

Live CD45+ immune cells from the dermis was isolated by FACS at early, mid and late telogen (10,000 for each condition), captured on a microfluidic chip, and processed for single-cell RNA sequencing with the 10X Genomics Chromium 3′ Solution platform. cDNA synthesized by this method was amplified and sequenced on an Illumina NextSeq and the data deposited in GEO (GSE108709). Cells with < 500 or > 2000 genes were excluded from analysis, as were cells with > 10^5 UMIs (reflecting doublets) or mitochondrial genes > 0.8% (reflecting dying cells). 1186 highly variable genes were identified based on their average expression and variance, and used for clustering analysis. Principle component analysis (PCA) on variable genes was performed by JackStraw analysis to identify significant PCs ($p < 0.05$), and t-Distributed Stochastic Neighbor Embedding (t-SNE) plots were made based on the first 28 PCs for all immune cells at all time points, and 10 PCs for just the macrophages at P45. Further analyses and presentation of data was performed with the Seurat R package (https://satijalab.org/seurat/install.html).

QUANTIFICATION AND STATISTICAL ANALYSIS

Hair Cycle Analysis

Quantification of anagen initiation was carried out by the darkening of the dorsal skin of C57BL/6 mice, an event that is closely coupled to anagen induction. Anagen quantification was performed using threshold analysis of the dorsal skin color in ImageJ, since darkening of the skin due to melanogenesis is coupled closely to anagen progression. Yellow boxes in Figures denotes the field selected for threshold analysis in ImageJ to measure the Anagen Induction Index.

Statistical Analysis

In the Figure Legends, "n" refers to number of mice, while "N" refers to number of cells. Animal and *in vitro* experiments had a minimum of 2 replications, specified in the Figure Legends.

Statistical analyses for animal and *in vitro* experiments were performed using the Graphpad Prism software. Student's unpaired t test was performed for normally distributed data. A two tailed paired t test was used where applicable. No statistical method was used to predetermine sample size. The experiments were not randomized. The investigators were not blinded to allocation during experiments or outcome assessment. For single-cell RNA sequencing and Enrichr data, p values were obtained from the Seurat R package and the online Enrichr program, respectively, and were not modified.

DATA AVAILABILITY

The accession number for the single-cell RNA sequencing data reported in this study is NCBI GEO: GSE108709.